Early-Stage Melt-Rock Reaction in a Cooling Crystal Mush Beneath a Slow-Spreading Mid-Ocean Ridge (IODP Hole U1473A, Atlantis Bank, Southwest Indian Ridge)

Alessio Sanfilippo [1,2,3]*, Christopher J. MacLeod [4], Riccardo Tribuzio [2,3], C. Johan Lissenberg [4] and Alberto Zanetti [5]

[1] Dipartimento di Scienze della Terra e dell'Ambiente, Universita' di Pavia, Pavia, Italy, [2] Graduate School of Natural Science and Technology, Kanazawa University, Kanazawa, Japan, [3] Istituto Geoscienze e Georisorse, Pavia, Italy, [4] School of Earth and Environmental Sciences, Cardiff University, Cardiff, United Kingdom, [5] National Research Council, Roma, Italy

Microtextural and chemical evidence from gabbros indicates that melts may react with the crystal framework as they migrate through crystal mushes beneath mid-ocean ridges; however, the importance of this process for the compositional evolution of minerals and melts remains a matter of debate. Here we provide new insights into the extent by which melt-rock reaction process can occur in oceanic gabbros by conducting a detailed study of cryptic reactive melt migration as preserved in an apparently unremarkable, homogeneous olivine gabbro from deep within a section of the plutonic footwall of the Atlantis Bank core complex on the Southwest Indian Ridge (International ocean discovery program Hole U1473A). High-resolution chemical maps reveal that mineral zoning increases toward and becomes extreme within a cm-wide band that is characterized by elevated incompatible trace element concentrations and generates extreme more/less incompatible element ratios. We demonstrate that neither crystallization of trapped melt nor diffusion can account for these observations. Instead, taking the novel approach of correcting mineral-melt partition coefficients for both temperature and composition, we show that these chemical variations can be generated by intergranular reactive porous flow of a melt as it migrated through the mush framework, and whose composition evolved by melt-rock reaction as it progressively localized into a cm-scale reactive channel. We propose that the case reported here may represent, in microcosm, a preserved snapshot of a generic mechanism by which melt can percolate through primitive mafic (olivine gabbro) crystal mushes, and be modified toward more evolved compositions via near-pervasive reactive transport.

Keywords: melt-rock reaction, reactive porous flow, lower oceanic crust, mineral zoning, South West Indian ridge

INTRODUCTION

Seismic investigations of mid-ocean ridges have shown that the large, km-scale melt-filled magma chambers originally inherent in ophiolite-derived models do not exist: at even the most magmatically robust fast-spreading ridges most of the lower ocean crust beneath the ridge axis transmits shear waves and is therefore largely solid, albeit normally with a tiny melt-rich lens or sill ≤10 s of meters thick present at the very top of the lower crust; instead, it is now generally believed that the broader lower crustal region must be comprised of a "crystal mush", apparently consisting of no more than a few percent interstitial melt overall (e.g. Detrick et al., 1987; Sinton and Detrick, 1992). At slower-spreading ridges, below ~50 mm/yr, even this small axial melt lens is not normally observed: detection of a comparable melt body in a few cases (e.g. Sinha et al., 1998) suggests it can exist but instead as a transient feature, although there are some indications that comparable crystal mush is present more widely in the lower crust beneath slower-spreading ridge axes (e.g. Singh et al., 2006). More broadly, the relative paucity of magma, together with observations such as the exposure of plutonic and/or mantle rocks on the seafloor near some slow-spreading mid-ridge axes, all leads to the recognition that melt delivery from the mantle at slower-spreading rates may be restricted in space and time, and is not always sufficient to generate or maintain a continuous magmatic crustal layer (Cannat et al., 2006). In such an environment, extensional tectonic processes are an integral part of the plate spreading process. Although subsequent geophysical experiments have identified small, sill-like melt bodies within the deeper lower crustal region beneath faster-spreading mid-ocean ridges (e.g., Marjanovic et al., 2014), the mechanisms of formation of the crystal mush, and the igneous processes that generate it, are poorly understood. From an igneous perspective, it is however agreed in broad terms that the magmatic lower crustal crystal mush must ultimately form by solidification of successive magma batches that somehow intrude, underplate and dissect existing crystal frameworks. At slower spreading ridges, this accretionary process is likely to be further complicated by physical and chemical interactions between different magmatic intrusions injected into an actively deforming environment (Dick et al., 2019b).

Several authors have suggested that when fresh injections of hot, primitive magma are intruded into a host rock they provide enough heat to melt the host minerals to some degree (Bédard et al., 2000; Leuthold et al., 2014; Coumans et al., 2016). Crustal melts can be produced and assimilated within the actively forming crustal mushes, leading to fundamental changes in melt (e.g., DePaolo, 1981; Solano et al., 2014; Jackson et al., 2018) and crystal compositions (Eason and Sinton, 2009). Furthermore, extensive reaction between interstitial liquid and host may also occur when chemically evolved melts migrate upwards, driven by buoyancy, compaction, deformation, or a combination thereof (Natland and Dick, 2001; Lissenberg et al., 2013, 2019). The equilibration between minerals and migrating melts leads to changes in mineral and melt chemistry at the reaction front, and these reactive melts crystallize new phases around partly resorbed pre-existing minerals, ultimately

modifying or even completely replacing the original crystal matrix (Coogan et al., 2000; Lissenberg and Dick, 2008; Suhr et al., 2008; Drouin et al., 2009; Drouin et al., 2010; Sanfilippo et al., 2015; Tamura et al., 2016 Ferrando et al., 2018). Whether leading to partial melting of the host rocks or selective dissolution of a crystal matrix, the assimilation of crustal material in the ascending magmas may be sufficiently efficient (Kvassnes and Grove, 2008; Yang et al., 2019) to potentially control the major- and trace element budgets of the melts erupted at the surface (e.g., Lissenberg and Dick, 2008; Lissenberg and MacLeod, 2016; Sanfilippo et al., 2016; Jackson et al., 2018; Renna et al., 2018; Lissenberg et al., 2019).

Textural evidence for reactive melt migration processes is widely preserved in abyssal and ophiolitic gabbros, and generally includes: 1) large poikilitic clinopyroxene (Cpx) locally containing resorbed olivine (Ol) and plagioclase (PL) chadacrysts (Blackman et al., 2006; Lissenberg and Dick, 2008; Sanfilippo and Tribuzio, 2013; Leuthold et al., 2014; 2018); 2) resorbed cores with higher An compared to the rim compositions in cumulus Pl (Lissenberg et al., 2013, Lissenberg et al., 2019; Lissenberg and MacLeod, 2016); 3) complex intergrowths of irregular Cpx commonly containing small (<100 μm) blebs of magmatic amphibole (Amp), oxides and orthopyroxene (Opx) (Tribuzio et al., 1999; Coogan et al., 2001; Dick et al., 2002; Beard et al., 2004; Lissenberg and MacLeod, 2016); and 4) Cpx-Amp symplectites (Lissenberg and MacLeod, 2016). However, Lissenberg and MacLeod (2016) recently provided evidence for reactive porous flow that was nearly undetectable from a textural perspective. They used Ti–Cr element mapping to show that chemical zoning characterizes the crystals of primitive olivine gabbros that otherwise possess an unremarkable, apparently well-equilibrated cumulus texture, and hypothesized that the chemical changes in minerals from these samples could be produced by reaction with migrating melts. The cryptic nature of the reaction was attributed to the fact that the reacting melt was at relatively high temperature, similar to that at which the original crystal framework was formed, and hence the reaction products were mineralogically similar to the original cumulus assemblage. If reactive melt flow can induce significant geochemical exchange in a cumulate system whilst leaving no characteristic textural signature in its wake, the process may be far more extensive and widespread in mafic cumulate systems than hitherto supposed. However, there is only very limited data to test this.

In this contribution we perform a detailed case-study of cryptic reaction between a crystal matrix and a migrating melt, developing a quantitative understanding of reactive porous flow at high temperatures (>1,050°C). We focus on an apparently mundane, texturally homogeneous olivine-gabbro from the plutonic lower crustal section of the Atlantis Bank oceanic core complex Southwest Indian Ridge; IODP Hole U1473A; (MacLeod et al., 2017). We will demonstrate that this key sample preserves evidence for a number of igneous processes that we argue are of broader significance at mid-ocean ridges and for mafic plutonic systems more generally. For the first time, we integrate high-resolution, thin section-scale chemical maps with detailed *in situ* mineral major- and trace-element analyses, to document a profound–yet petrographically undetectable–variability
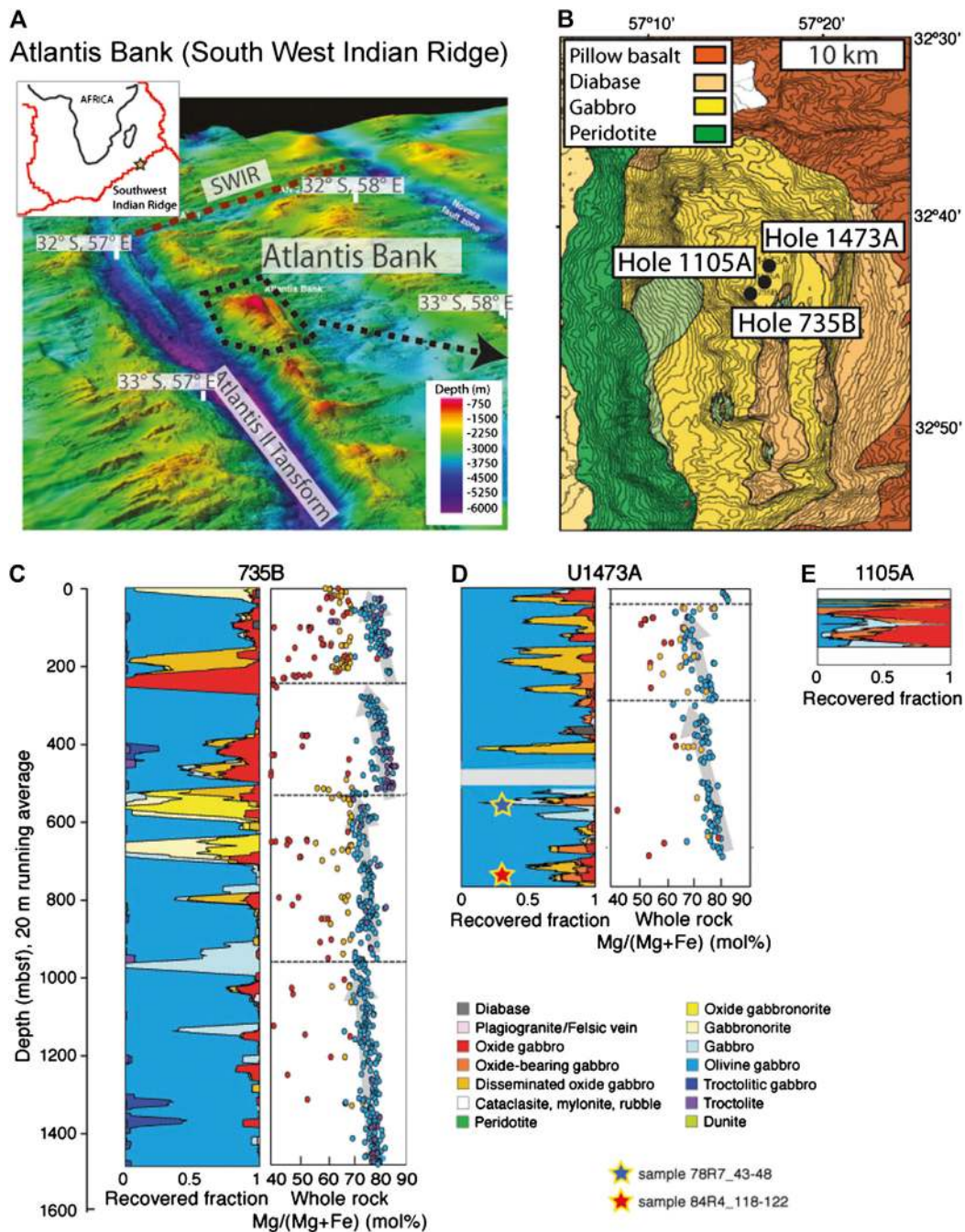
FIGURE 1 | (A) Location and bathymetric map of the Atlantis II Fracture Zone in the Southwest Indian Ridge and (B) and detail of the Atlantis Bank core complex showing the location of Holes 1105A, 735B and U1437A (C) Stratigraphic columns representing running averages of lithological intervals plotted against depth in Holes 735B, U1473A and 1105A. Whole rock Mg/(Mg + Fe) (mol%) compositions of samples from Hole 735B and U1473A are also reported, defining distinct geochemical units (modified from MacLeod et al., 2017). The location of samples U1473A-78R-7_43–48 and U1473A-84-R4_118–122 is also indicated.

in mineral composition and zoning throughout the sample, localized within a highly modified cm-scale "reaction band" within the sample. We show that the reaction band most likely represents a high local melt flux channel, and demonstrate that the mineral chemical modifications throughout the sample are explained by dissolution-reprecipitation melt-rock reactions that

occurred under decreasing temperature conditions as melt migrated through the host crystal framework. If evidence for near-pervasive reactive porous melt migration is preserved in even the most mundane sample of primitive olivine gabbro, which we take as representative of the early-formed crystal mush framework in magma bodies beneath mid-ocean ridges–and

this evidence is otherwise invisible without modern high-resolution chemical imaging and mapping–then it follows that reactive porous melt percolation through mushes may be a far more prevalent mechanism of melt transport and modification in the lower ocean crust than presupposed. Our study also highlights that the kind of detailed investigation presented here, integrating high-resolution, thin section-scale chemical maps with chemical profiles, are a first-order necessity to illuminate the chemical evolution of crystal mushes (Lissenberg & MacLeod, 2016), and to allow more meaningful comparison of the natural cases with theoretical models (e.g. Jackson et al., 2018).

LOWER OCEANIC CRUST AT HOLE U1473A, ATLANTIS BANK OCEANIC CORE COMPLEX SOUTHWEST INDIAN RIDGE

The Southwest Indian Ridge (SWIR) is a slow-to ultraslow-spreading mid-ocean ridge, spreading approximately N-S at a full spreading rate of 14 mm/yr. For much of its length the ridge trends SW-NE, oblique to its spreading direction. Between ~52°E and 60°E the Southwest Indian Ridge axis is offset by a series of prominent, long-offset N-S striking transform faults, among which the Atlantis II Transform (at 57°E) has an offset of 200 km. On a transverse ridge east of the transform valley and ~80 km south of the present axis lies the Atlantis Bank (Figure 1A), a large oceanic core complex that exposes a tectonic window of deep crustal and lithospheric mantle exhumed in the footwall of an 11–13 Myr old oceanic detachment fault (e.g., Dick et al., 1991; Dick et al., 2000). Atlantis Bank is comprised of a >400 km^2 gabbro massif overlying serpentinized mantle peridotites that crop out along the slopes of the eastern transform wall (Dick et al., 2019a). The shallowest part of Atlantis Bank is at ~700 m water depth and consists of a wave-cut platform rimmed by a thin limestone cap. Here, the top of the basement consists of amphibolitised gabbro mylonite generated by detachment faulting (MacLeod et al., 1998). Previous Ocean Drilling Program (ODP) operations at Atlantis Bank drilled the 1,508 m deep Hole 735B, and 150 m deep Hole 1105A, both recovering long sections of gabbro sensu lato (Dick et al., 1991; Dick et al., 2000; Pettigrew et al., 1999). Recently, International Ocean Discovery Program (IODP) Expedition 360 drilled a further deep hole, at Site U1473, located ~2.2 and 1.4 km north-northeast and north of Hole 735B and 1105A respectively (MacLeod et al., 2017; Figure 1B).
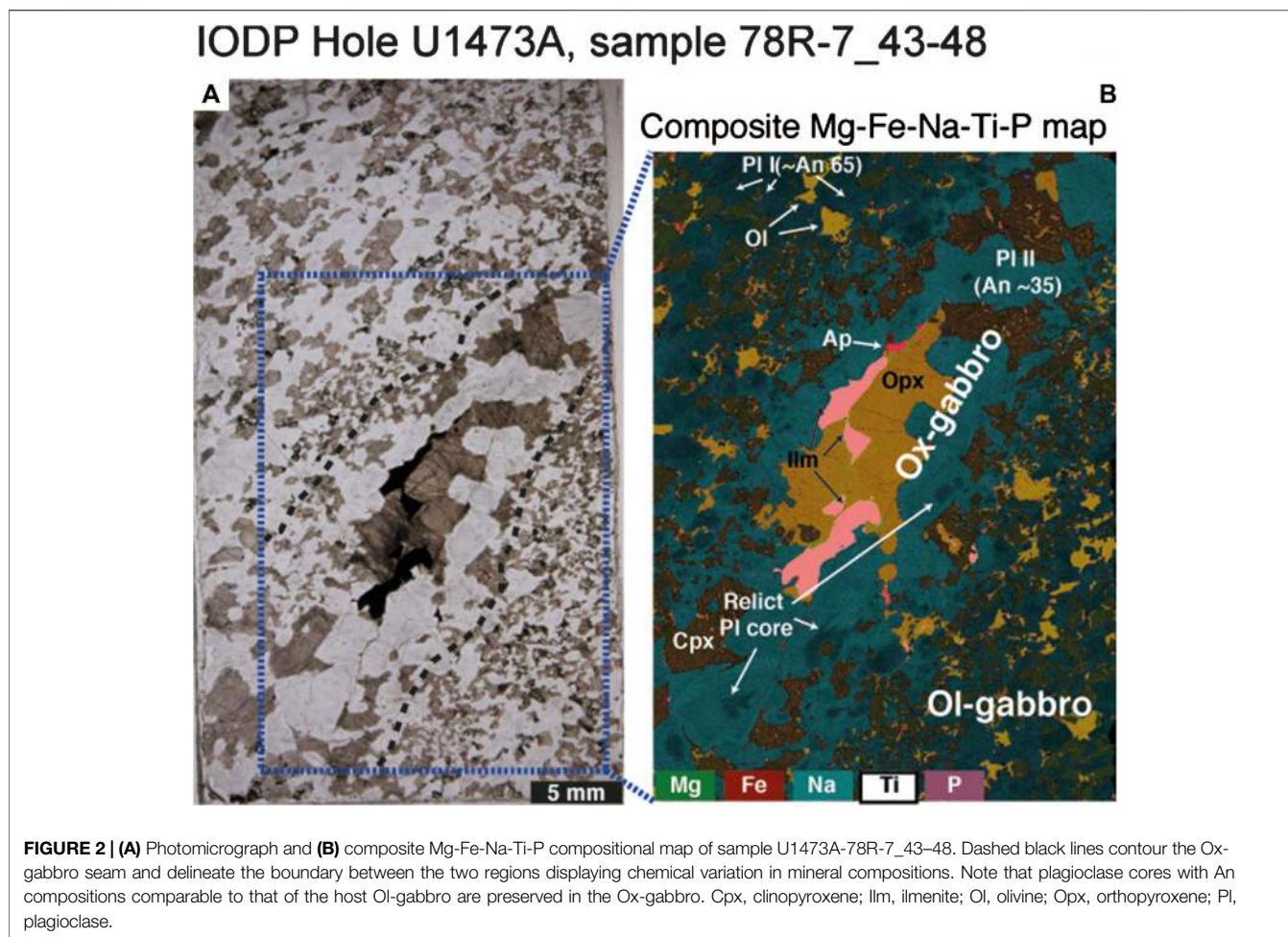
Eighty-nine cores were drilled at Hole U1473A (32°42.3622S 57°16.6880′E, 710.2 m water depth; MacLeod et al., 2017), supplemented by five further cores during engineering Expedition 362T, to a current total depth of 809.4 m below seafloor (mbsf; Blum et al., 2017). Overall recovery was 44%, relatively low in the upper part of the hole because of the presence of a fault zone, though markedly higher, at ~96%, in the lowermost few hundred meters. Similar to the previous drill holes at Atlantis Bank, the section drilled at IODP Hole U1473A is mainly composed of olivine (Ol) gabbro (Ol > 5 vol%), interspersed with more evolved oxide (Ox)-bearing varieties, and cut by felsic veins and rare diabase dykes

(MacLeod et al., 2017; Figure 1). Most of the gabbros show textural evidence for crystal-plastic deformation, ranging from hyper-solidus to granulite and amphibolite grade facies, as a consequence of the deformation event related to the detachment faulting and exhumation of the plutonic basement.

The principal lithology is coarse-to medium-grained olivine gabbro (76.5%); only 5.1% of Hole U1473A is gabbro (<5 vol% olivine) sensu stricto (MacLeod et al., 2017). Primary magmatic textures throughout the hole are in many instances partially obscured by crystal-plastic deformation, typically expressed in the form of undulose extinction of cumulus phases and/or variable plagioclase neoblast formation, but extending in some instances to the development of mylonitic or ultramylonitic textures (MacLeod et al., 2017). Completely undeformed gabbros are preserved in only a few intervals: from petrographic examination we observe some degree of plagioclase neoblast development at grain boundaries in most of those units previously described as "undeformed" on the basis of macroscopic description (crystal-plastic fabric "0": MacLeod et al., 2017). In the few samples in which recrystallization is absent in thin section the rocks appear generally equigranular, and with highly variable grain sizes ranging from fine-grained to pegmatitic. Magmatic fabrics are rare but, where visible, are defined by the preferred orientation of Pl and, in some instances, by the occurrence of decimetre-scale igneous layering defined predominantly by grain-size variation.

The Ol-gabbros are interspersed with evolved Ox-bearing (Ox > 1 vol%) lithologies, which include disseminated Ox-gabbro (Ox 1-2 vol%), Ox-bearing gabbro (Ox 2-5 vol%) and Ox-gabbro (Ox > 5 vol%) that constitute 9.5, 3.7, and 3.7% of the hole, respectively. Ox-bearing rocks tend to be slightly more deformed than the host Ol-gabbros and are widespread in the entire section at Hole U1473A (MacLeod et al., 2017), whereas they tend to be highly localized at several deformed horizons in shallower levels of Hole 735B (Ozawa et al., 1991). Finally, different generations of felsic rocks (i.e., leucodiorite, diorite, quartz diorite, trondhjemite, and tonalite) crosscut the Ol-gabbros in the form of irregular patches and veins. The felsic veins locally crosscut the foliation, although they may themselves be internally deformed. Felsic material makes up ~1.5 vol% of the core and tends to be concentrated in specific zones, within which it appears to have been formed either as intrusions of a late-stage melt or by crystallization of melts produced by local gabbro anatexis (e.g., Koepke et al., 2007; Nguyen et al., 2018).

Taken as a whole, the igneous stratigraphic relationships and range of lithologies recovered in Hole U1473A are similar to those encountered in the previous holes at Atlantis Bank, but cannot be compared directly. Altogether, the respective sequences show the absence of any direct correlation or systematic variation, either laterally (on a km-scale) or vertically (on a 100 s of meter scale), indicating that accretion of the lower crust in this region was governed by a complex, continual interplay between magmatic intrusion, crystallization and hyper-solidus to high-temperature sub-solidus deformation. As separately deduced from the plutonic complex sampled at Hole U1309D at Atlantis Massif (Mid-Atlantic Ridge), the only other long section drilled into an oceanic core complex thus far (Blackman et al., 2006; Blackman

FIGURE 2 | (A) Photomicrograph and **(B)** composite Mg-Fe-Na-Ti-P compositional map of sample U1473A-78R-7_43–48. Dashed black lines contour the Ox-gabbro seam and delineate the boundary between the two regions displaying chemical variation in mineral compositions. Note that plagioclase cores with An compositions comparable to that of the host Ol-gabbro are preserved in the Ox-gabbro. Cpx, clinopyroxene; Ilm, ilmenite; Ol, olivine; Opx, orthopyroxene; Pl, plagioclase.

et al., 2011), the metre-scale heterogeneity in composition and texture suggests that the plutonic lower crust at slow-spreading ridges forms through the successive accretion of episodic "nested" intrusions to form an heterogeneous gabbroic layer (e.g., Cannat and Casey, 1995; Grimes et al., 2011; Rioux et al., 2016).

CHEMICAL EVIDENCE FOR REACTIVE MELT MIGRATION PROCESSES IN THE ATLANTIS BANK LOWER OCEANIC CRUST: PREVIOUS STUDIES

Previous authors have proposed that gabbros from Atlantis Bank experienced some degree of porous melt-crystal interaction (e.g., Dick et al., 1991, Dick et al., 2000; Gao et al., 2007; Lissenberg and MacLeod, 2016; MacLeod et al., 2017). Most obvious evidence for this process is the occurrence of centimetre-to decimetre-scale evolved Ox-rich gabbro patches and veinlets that cross-cut primitive Ol-gabbros, interpreted as localized zones of crystallization of highly evolved, Fe-Ti oxide-saturated melts (Dick et al., 1991; Dick et al., 2000; Ozawa et al., 1991; Natland and Dick 2001). Recently, Lissenberg and MacLeod

(2016) used chemical maps and trace element profiles of petrographic thin sections from Hole 735B to propose that some mylonitic Ox-gabbro bands formed by a process of hybridization of a former Ol-gabbro that had been converted into an Ox-rich lithology by melt-rock reaction (see also Ozawa et al., 1991).

The same textural relationships between Ox- and Ol-gabbros are observed in Hole U1473A and the same reactive melt migration processes may also be inferred (see also MacLeod et al., 2017; Dick et al., 2019b). We report by way of example sample 360-U1473A-78R-7, 43–48 cm (**Figure 2**), a typical undeformed olivine gabbro notable in hand specimen principally for containing a narrow (12 mm-wide) band or pocket of coarser-grained Ox-gabbro (**Figure 2A**). Such primitive/evolved mineralogical relationships, with olivine and Fe-Ti oxide in close proximity, are widespread and unremarkable both in the Hole U1473A section (see MacLeod et al., 2017) and in gabbros from elsewhere in Atlantis Bank (Dick et al., 1999; Dick et al., 2019a). The contact between the two lithologies is diffuse, and ill-defined in both hand specimen or petrographic thin section (**Figure 2A**). The compositional difference between the two lithologies becomes obvious only in the combined
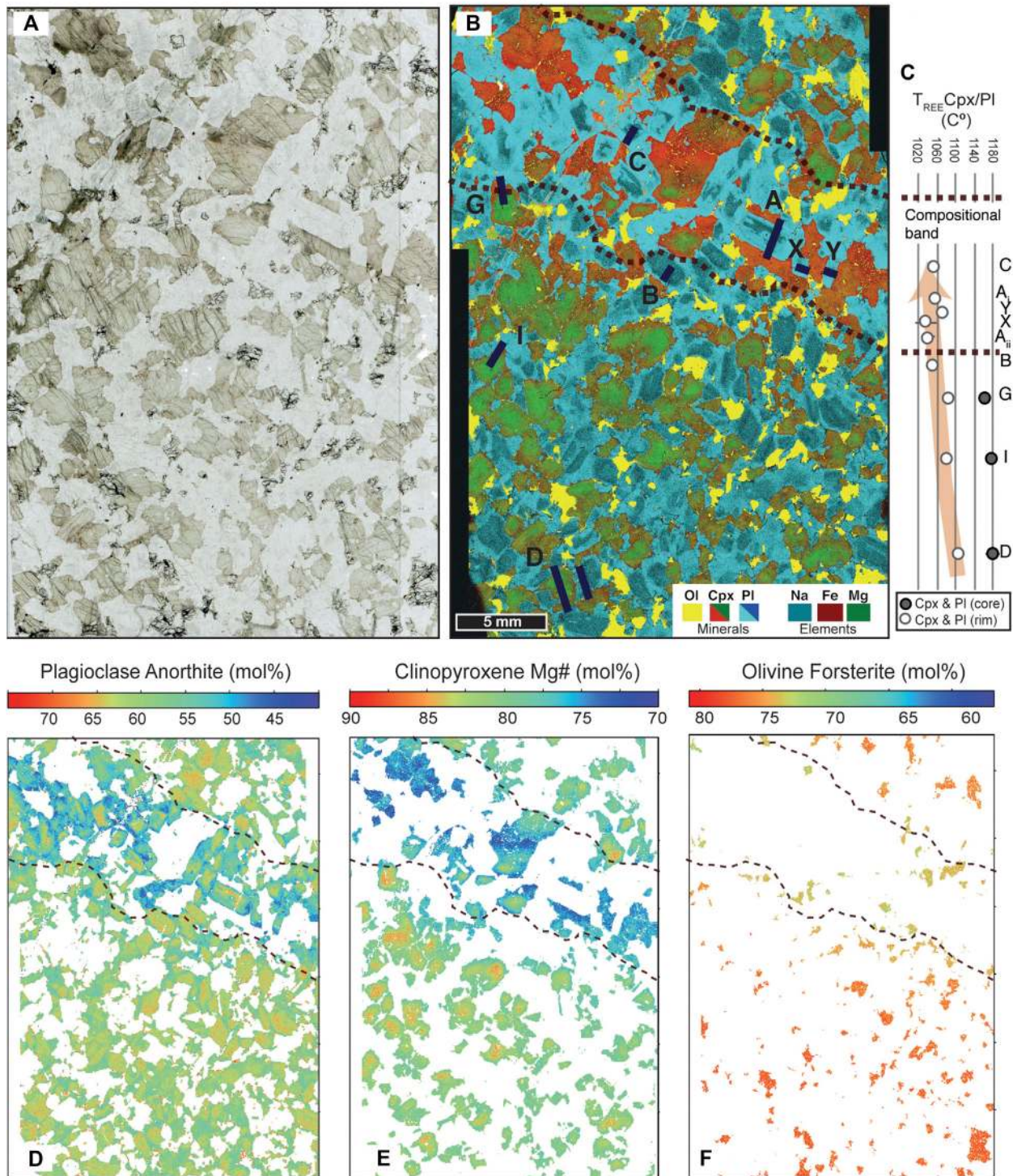
FIGURE 3 | (A) photomicrograph of sample U1473A-84R-4_118–112. The sample has a granular, equilibrated texture, with negligible crystal plastic deformation, and lacking petrographic evidence for mineral reactions. The composite Mg-Fe-Na-Ti element map in **(B)** however reveals a compositional band within which plagioclase and clinopyroxene have more evolved compositions. Corroded plagioclase cores are preserved in the band. **(C)** Variation of the Cpx-Pl equilibration temperatures using the Cpx-PlREE-Y geothermometer of Sun et al. (2017). Note that Cpx-Pl equilibration temperatures tend to decrease toward the compositional band. Core temperatures were not calculated within the band due to the lack of clinopyroxene having core compositions. **(D)** Anorthite maps in plagioclase **(E)** Fo map in olivine and **(F)** Mg# maps in clinopyroxene calculated using the Quack software. Black dashed lines in **(B)**, **(D)**, and **(F)** delineate the compositional band. Also indicated in **(B)** are the areas selected for the detailed trace element determination and the geochemical traverses (black lines).

element map (**Figure 2B**; see Cryptic Chemical Variations in an Apparently Homogeneous Olivine-Gabbro below) from which it is evident that the minerals in the Ox-gabbro band have substantially more evolved compositions (Pl An ~35, Cpx Mg# ~65) than the host (Pl An~65, Cpx Mg#~82). However, we note the occurrence of relict, partially resorbed cores of high An plagioclase which, coupled with the gradational decrease of the An content in the Pl of the host Ol-gabbros, is hard to explain by the simple *in situ* crystallization of a melt pocket; instead, it suggests that the Ox-gabbros formed by the migration of chemically evolved (Fe-Ti-rich) melt into an existing crystal matrix of primitive Ol, Pl and Cpx. This deduction is directly comparable to that inferred from previous studies on Ox-gabbros from Hole 735B Ox-gabbros (e.g., Ozawa et al., 1991; Lissenberg and MacLeod, 2016).

Whether reactive porous flow is also a significant process in the Ol-gabbros that are the primary constituent of the section at Atlantis Bank (~77%) and regarded as the primary crystal mush framework, is more difficult to assess. Gao et al. (2007) previously documented strong core–rim enrichment in incompatible elements of Cpx in the Hole 735B Ol-gabbros, which display over-enrichments in highly incompatible trace elements relative to less incompatible trace elements (i.e., Ce to Y; Zr to Nd). These authors showed that enrichments in Zr and LREE are more extreme than those expected in fractional crystallization models, and cannot be explained by crystallization of trapped melt *in situ* (Bedard 1994). Similar trace element zoning patterns were documented by Lissenberg and MacLeod (2016) in a core–rim traverse of a large (8 mm) Cpx from an apparently homogeneous Ol-gabbro. They measured the core–rim distributions of several trace elements (i.e., Cr, Ti, Y, Yb, Nd, Zr, Ce and La), and noted selective over-enrichment from core to rim in La, Zr and Ce (all reaching a factor of ~30x enrichment from core to rim) and, furthermore, strong concomitant increases in Ce/Y and Zr/Nd ratios. Together with the preservation of Mg-Fe chemical zoning, these observations led the same authors to conclude that the grain-scale over-enrichment both in incompatible trace element abundances and trace element ratios in Ol-gabbro resulted from dissolution–reprecipitation reactions between migrating melts and a primitive crystal mush.

CRYPTIC CHEMICAL VARIATIONS IN AN APPARENTLY HOMOGENEOUS OLIVINE-GABBRO

Sample Selection and Analytical Methodology

In this study we hereinafter focus on an apparently unremarkable "typical" coarse-grained olivine gabbro, in which the potentially complicating effects of deformation are absent and which lacks any visible textural evidence of melt-rock interaction. This sample (360-U1473A-84R-4, 118–122 cm; 746 m below seafloor; **Figure 3**) has some of the most primitive mineral compositions encountered at Hole U1473A and contains an extremely low proportion of accessory phases, so much so that it was initially selected for study

as a typical representative of the predominant olivine gabbro facies and hence pre-supposed to be the least modified representative of the original cumulate crystal mush. Oxides and apatite are found only as a few <0.1 mm grains, and Amp and Opx are absent completely. Cpx and Pl have sub-ophitic texture, whereas Ol is typically subhedral to interstitial, although a few fine-grained Ol chadacrysts are locally included in Cpx.
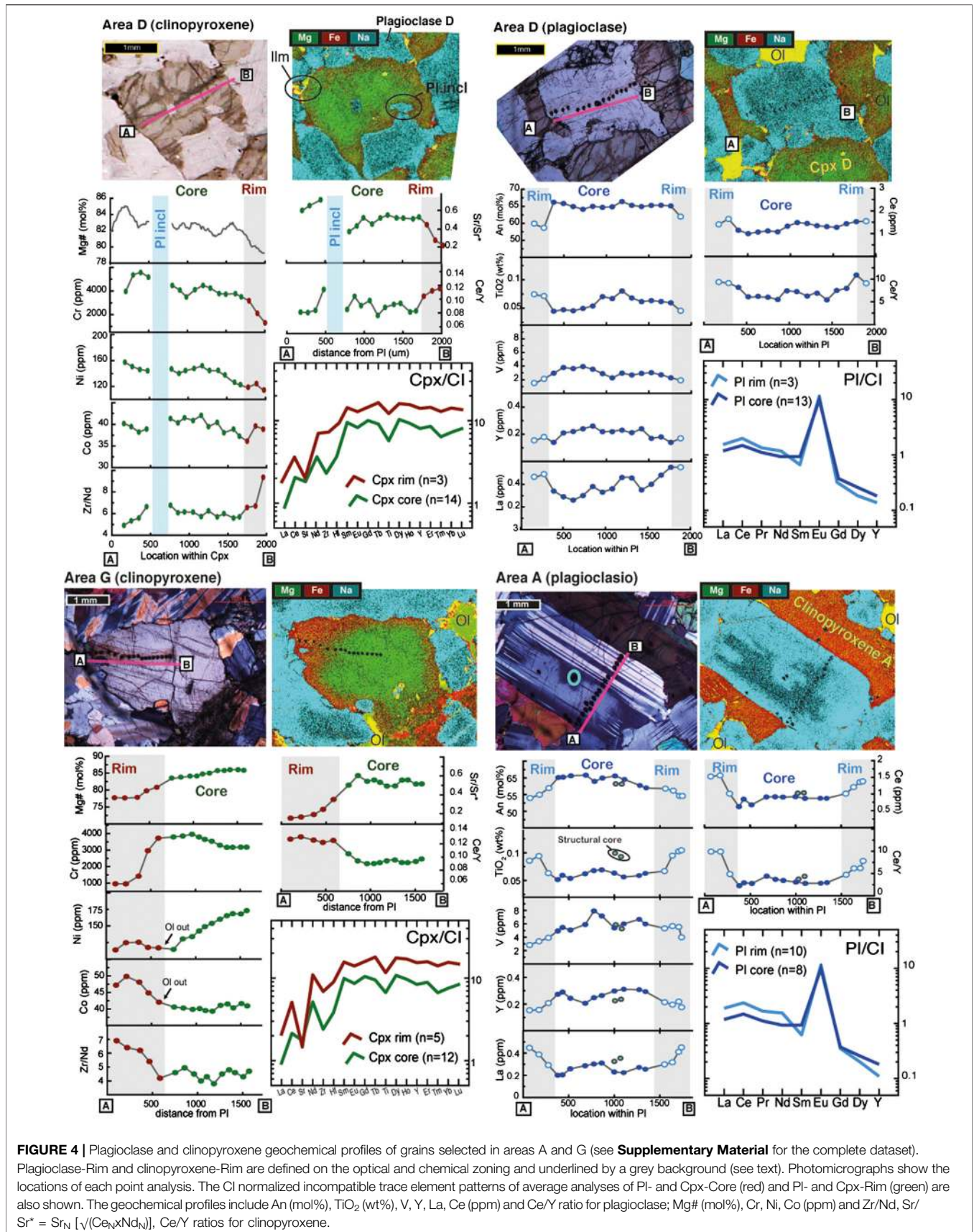
We acquired chemical maps of whole thin sections of the sample using a Zeiss Sigma HD field emission gun SEM installed at Cardiff University. This machine is equipped with dual 150-mm^2 Oxford Instruments X-Max^N energy dispersive silicon drift detectors, which enable high count rates (>1,000,000 cps) and rapid acquisition of quantitative element maps of all phases e.g. Pl anorthite and Cpx Mg#, in this case at 10 μm step ("pixel") size. The data were background-corrected using Oxford Instruments AZtec software prior to the production of element maps. Mineral major element compositions (An in Pl, Mg# in Cpx and Fo in Ol) were quantified from the element maps using the approach of Loocke (2016).

Major element compositions of points along a series of detailed mineral transects were separately acquired using a JEOL JXA-8200 electron microprobe located at Dipartimento di Scienze della Terra, Universita' degli Studi di Milano (Italy). Conditions of analyses were 15 kV accelerating voltage and 15 nA beam current. Counting time was 30 s on the peak and 10 s on the backgrounds. Natural standards were utilized and data reduction was carried out using the CITZAF package. Pl, Cpx and Ol compositions as deduced from the element maps (**Figure 3**) differ from the point analyses by ≤ 2% in An, Mg# and Fo.

Trace element compositions of clinopyroxene and plagioclase from these transects were obtained using Laser Ablation Inductively Coupled Plasma Mass Spectrometry (LA-ICP-MS) at C.N.R., Istituto di Geoscienze e Georisorse (Unita' di Pavia; **Supplementary Tables S1 and S2**). The probe consists of a PerkinElmerSCIEX ELAN DRC-e quadrupole mass spectrometer coupled with an UP213 deep-UV YAG Laser Ablation System (New Wave Research, Inc.). The laser was operated at a repetition rate of 10 Hz, with 213 nm wavelength and a fluence of ~9.5 J/cm^2. Helium was used as carrier gas and was mixed with Ar downstream of the ablation cell. Spot diameter ranged from 50 to 100 microns. Data reduction was performed offline using the GLITTER software. For this study, the NIST SRM 610 synthetic glass standards was used as external standard, and CaO as internal standard. Precision and accuracy of the REE concentration values were assessed through repeated analysis of the BCR2-g standard to be better than ±7% and ±10%, respectively, at the ppm concentration level.

Results

High-resolution chemical maps show that Pl and Cpx across the entire thin section exhibit prominent chemical zoning, characterized by an overall decrease in Pl An and Cpx Mg# from the cores to the rims of most minerals (**Figure 3**). Even more noteworthy is that the chemical maps also document an otherwise invisible increase in the extent of zoning toward an inclined, centimetre-wide band, within which Pl is characterized by

FIGURE 4 | Plagioclase and clinopyroxene geochemical profiles of grains selected in areas A and G (see **Supplementary Material** for the complete dataset). Plagioclase-Rim and clinopyroxene-Rim are defined on the optical and chemical zoning and underlined by a grey background (see text). Photomicrographs show the locations of each point analysis. The CI normalized incompatible trace element patterns of average analyses of Pl- and Cpx-Core (red) and Pl- and Cpx-Rim (green) are also shown. The geochemical profiles include An (mol%), TiO$_2$ (wt%), V, Y, La, Ce (ppm) and Ce/Y ratio for plagioclase; Mg# (mol%), Cr, Ni, Co (ppm) and Zr/Nd, Sr/Sr* = Sr$_N$ [$\sqrt{(Ce_N \times Nd_N)}$], Ce/Y ratios for clinopyroxene.
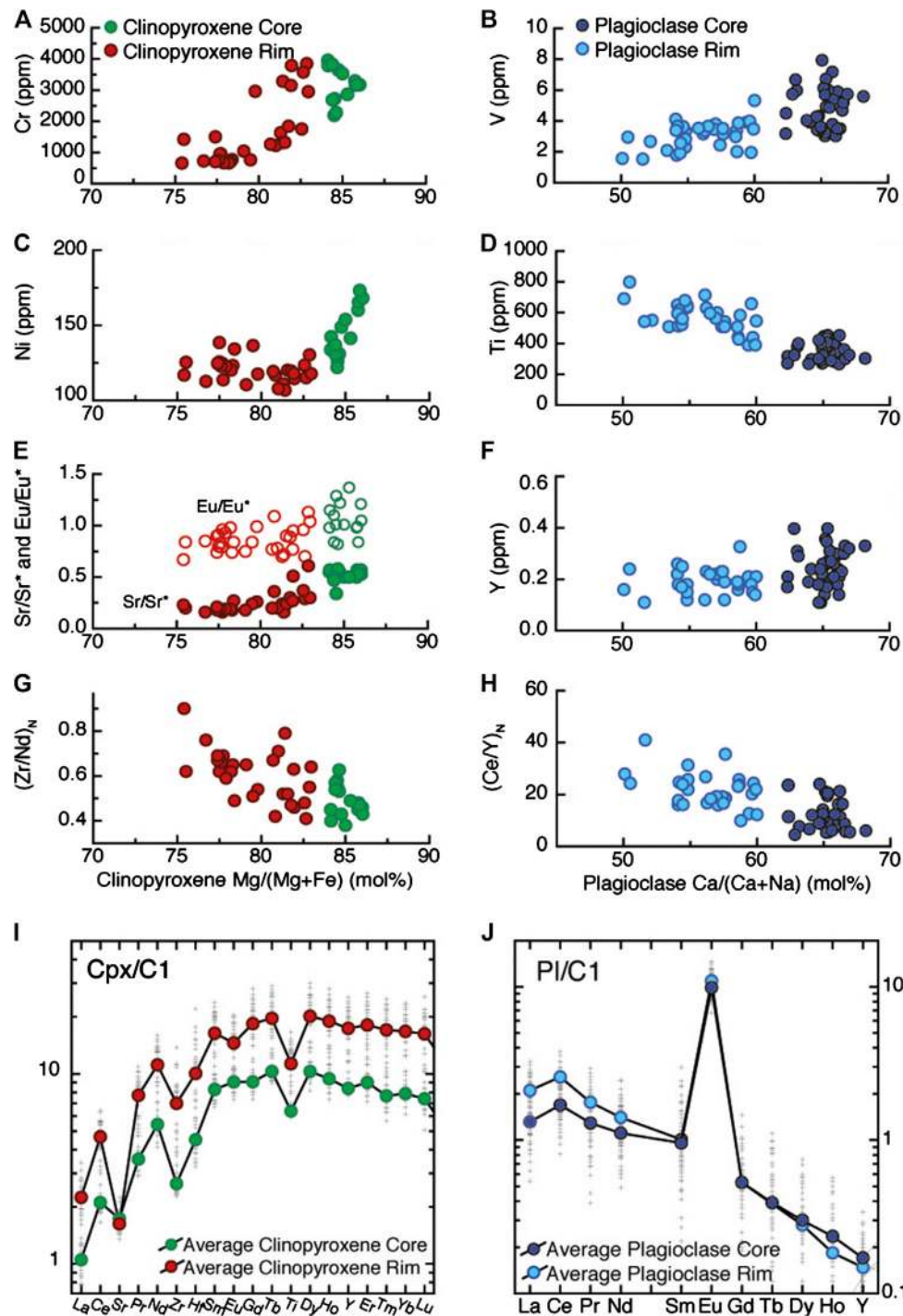
FIGURE 5 | General trace element variability of clinopyroxene and plagioclase from the entire thin section. Clinopyroxene (Cpx) Mg/(Mg + Fe) (mol%) vs. Cr, Ni (ppm), Sr/Sr* = $Sr_N [\sqrt{(Ce_N \times Nd_N)}]$, Eu/Eu* = $Eu_N [\sqrt{(Sm_N \times Gd_N)}]$ (Zr/Nd)$_N$ ratios. Plagioclase (PL) Ca/(Ca + Na) (mol%) vs. V, Ti, Y (ppm) and (Ce/Y)$_N$ ratio. Chondrite (C1)-normalised (Anders and Ebihara, 1982) incompatible trace element patterns of each point (grey cross) and average Cpx-Core and Pl-Core and Cpx-Rim and Pl-Rim are also depicted. The different generations of Pl and Cpx are defined on the basis of the chemical profiles in **Figure 4** and **Supplementary Figure S1**.

irregular, partly corroded An-rich cores surrounded by often euhedral, An-poor rims. As this band is approached Cpx tends to acquire a coarser grain-size and a poikilitic texture, at the same time becoming progressively enriched in Fe. Furthermore, the

magnitude of Fe-Mg zoning in Cpx of the Ol gabbro increases toward the band. Intra-grain Mg-Fe zoning is not obvious in Ol from the combined compositional map (**Figure 3A**) for reasons of color scaling, but the transition toward more fayalitic

compositions is clearly evident in the specific olivine composition map (**Figure 3E**). In addition, from the same figure it is clear that Ol is progressively less abundant, acquires irregular habits, and finally disappears toward the innermost part of the band. Critically, all of these coupled textural-compositional changes are gradual.

We investigate the variations in trace element concentrations and zoning characteristics of different individual Cpx and Pl grains, chosen on the basis of their location and of their major element chemical zoning characteristics determined from the element maps (**Figure 3B, D**). Cpx and Pl were selected in progressive proximity to the band (see locations in **Figure 3**). Two examples of Cpx and Pl are reported in **Figure 4**, as representative of the chemical zoning in this section; additional transects are reported in **Supplementary Figure S1** and listed in **Supplementary Tables S1 and S2**. The Cpx grains display a strong Fe-Mg zonation, with Mg# ranging from ~87 in the core to ~77 at the rim. The decrease in Mg# is coupled with a decrease in compatible elements such as Cr and Ni (ranging from ~3,500 to 1,000 ppm and from 175 to 125 ppm, respectively) and by corresponding increases in all incompatible elements. This is obvious from the chondrite-normalized (Anders and Ebihara, 1982) patterns depicted in **Figure 4**, which show Cpx rims having sub-parallel trace element patterns at progressively higher absolute concentrations, but a deep negative Sr anomaly compared to the Cpx cores. As typically reported in Cpx from other Ol-gabbros from Hole 735B (Gao et al., 2007; Lissenberg and MacLeod, 2016), a gradual enrichment in incompatible elements is present from the core toward rim, coupled with a concomitant increase in the ratios of more-incompatible/less-incompatible elements: for instance, Cpx cores have low and nearly constant Zr/Nd (~4), and Ce/Y (~0.09) ratios that increase toward the rim at 7 and 1.3, corresponding to core/rim enrichment factors of 1.7 and 1.4, respectively.

Major and trace element zoning is equally well developed and ubiquitous in Pl (**Figure 3B, E**). Plagioclase An content in all selected grains decreases from their cores to their rims. As with Cpx, the major element chemical zoning in Pl is associated with enrichments in the most incompatible elements (e.g., Ti, La or Ce) compared to the least incompatible (i.e., Y). This results in low and constant Ce/Y ratios in the Pl cores (~2.5), which gradually increase by up to 4 times toward the rims (Ce/Y ratios up to 10). As a consequence, the C1-normalized patterns of the Pl cores are relatively flat in LREE, whereas those of Pl rims show positive fractionations in LREE, and lower Gd, Dy and Y, compared to the Pl cores. The only exceptions are two small euhedral Pl grains included in a Cpx within the band, which have no An zoning and show compositions similar to the rims of the other minerals (see area X and Y in **Supplementary Figure S1**).

A generalized view of the chemical characteristics of these minerals is shown in **Figure 5**, in which Pl and Cpx "Rims" represent the spot analyses located within the band and mostly, but not only, localized at the rim of the minerals. Indeed, a fundamental observation is that chemical variations in Cpx and Pl are primarily localized in specific zones within the section (**Figure 3**). Away from the compositional band most of the sample comprises

crystals with thin rims of more evolved compositions; in contrast, minerals within the band are mainly composed of this rim composition, with small, often resorbed, cores compositionally similar to the host Ol-gabbro. Hence, what we labeled "Cpx-Cores" correspond to locations having Mg# > 83, and also characterized by high Cr and Ni and low TiO₂ and incompatible trace elements, contrasting with "Cpx-Rims" which are instead characterized by gradually higher incompatible trace element compositions, pronounced negative Sr anomalies, and high Zr/Nd and Ce/Y ratios. Following the same rationale we defined "Pl-Core" as those locations with An > 61, and generally having low Ti, nearly flat LREE, and higher Y concentrations compared to "Pl-Rim".
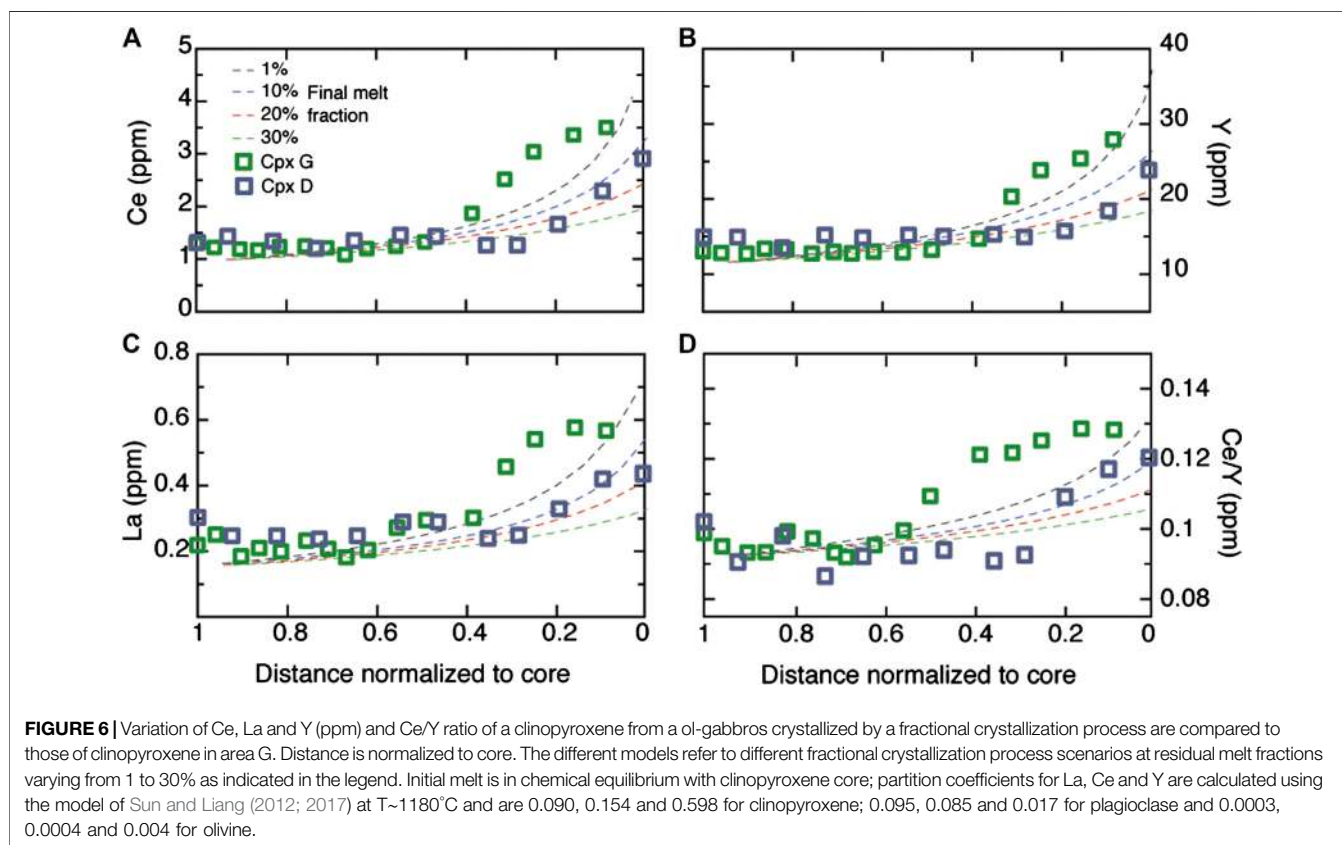
DISCUSSION

Origin of Trace Element Zoning: Trapped Melt, Diffusion or Reactive Porous Flow?

As more trace element mineral chemical studies of abyssal gabbros are being conducted, it is becoming clear that intra-crystal trace element zoning is a widespread phenomenon. Typically, transitions in composition from core to rim in Cpx are marked by a decrease in compatible elements (e.g. Cr), a deepening of Sr and Eu anomalies, and a general increase in incompatible elements (Coogan et al., 2000; Gao et al., 2007; Drouin et al., 2009; Lissenberg et al., 2013; Sanfilippo et al., 2015; Lissenberg and MacLeod, 2016). At the same time, Pl rims show enrichments in LREE, whereas HREE and Y exhibit slight decreases (Lissenberg et al., 2013; Coogan and O'Hara, 2015).

Several very different processes have been proposed thus far to explain such mineral trace element zoning patterns, with profoundly different implications for magmatic processes and the behavior of melts in igneous systems. They may be broadly summarized as: 1) melt entrapment *in situ*; 2) diffusional re-equilibration; and 3) reactive porous flow. We here examine each of these hypotheses in turn to explore whether they might explain the observations we have documented.

Melt Entrapment

The entrapment of small aliquots of melt within a crystal matrix can generate zoning as a result of the progressive fractional crystallization of trapped melt as the system cools. This zoning is characterized by an increase of incompatible elements from core to rim of a crystal, coupled with a decrease of compatible elements. This process of *in situ* melt entrapment has been traditionally and widely invoked to explain much of the major element chemical zoning in minerals from plutonic crustal rocks (e.g., Meyer et al., 1989; Elthon et al., 1992). Previous authors explored the ability of melt entrapment to account for such strong enrichments in abundances and increases in more incompatible/less incompatible element ratios (e.g. Coogan et al., 2000; Gao et al., 2007; Lissenberg et al., 2013; Sanfilippo et al., 2015). In each case these studies showed that increases e.g. Ce/Y, Zr/Nd from crystal core to rim (see **Figure 4**) are typically too large to be explained by any conventional fractional crystallization mechanism. We test this hypothesis again here for our specific example by exploring whether a fractional crystallization process

FIGURE 6 | Variation of Ce, La and Y (ppm) and Ce/Y ratio of a clinopyroxene from a ol-gabbros crystallized by a fractional crystallization process are compared to those of clinopyroxene in area G. Distance is normalized to core. The different models refer to different fractional crystallization process scenarios at residual melt fractions varying from 1 to 30% as indicated in the legend. Initial melt is in chemical equilibrium with clinopyroxene core; partition coefficients for La, Ce and Y are calculated using the model of Sun and Liang (2012; 2017) at T~1180°C and are 0.090, 0.154 and 0.598 for clinopyroxene; 0.095, 0.085 and 0.017 for plagioclase and 0.0003, 0.0004 and 0.004 for olivine.

is capable of reproducing the La, Ce and Y variations of the two detailed Cpx profiles we obtained (areas D and G). In **Figure 6** we model the behavior of clinopyroxene during closed-system fractional crystallization of an olivine gabbro with the same proportions as observed in our rock (Ol-Pl-Cpx 0.1:0.5:0.4), assuming a concentric spherical growth of clinopyroxene and crystal growth assumed to be proportional to the crystallization of the melt. The initial melt is in equilibrium with the core composition and the final melt fraction (i.e., the remaining fraction of melt during the crystallization of the rim) was chosen to vary between 1 and 30% to simulate different proportions of melt entrapment. Partition coefficients for Ol, Pl and Cpx are reported in the caption to **Figure 6**. We find that the decrease of melt fraction indeed causes a strong increase both in elemental concentrations and in Ce/Y ratios toward the rim; however, the observed zoning profiles cannot be fitted by any fractional crystallization process in a closed system. In particular, Cpx G, within the compositional band, shows increases in La and Ce concentrations and, in consequence, Ce/Y ratios, that are more rapid than can be accounted for by fractional crystallization. Only the rim composition of Cpx D, far from the band, seems to be intercepted by the fractional crystallization trends. Even so, fractional crystallization cannot account for the steep increase in e.g., Ce/Y between the core composition and the rim of this crystal (normalized distance of ~0.08–0.3; **Figure 6**); furthermore, if the rim data point did record fractional

crystallization, it would require a final melt fraction of <10% so to do. In consequence, more than 90% of the initial melt mass needs to have been entrapped in the cumulus matrix to explain such enriched compositions. To test whether the degree of fractionation implied is consistent with the textural and chemical characteristics of our sample we use a *MELTS* calculation (Ghiorso and Sack, 1995) starting with an average melt composition for the Southwest Indian Ridge basalts (Coogan et al., 2004). The *MELTS* model indicates that late-stage phases such as Ti-Fe oxides and orthopyroxene should start to crystallize as early as F~0.85 and, in agreement with experimental results (Feig et al., 2006; Koepke et al., 2018), further shows that these late phases should also be associated with pargasitic amphibole. This contrasts with the mineral assemblage of our sample, in which these interstitial phases are almost completely absent. Furthermore, >90% fractionation crystallization should generate a melt with Mg# of <30 mol%, which is inconsistent with the observed Mg# (~77 mol%) of the Cpx rim in chemical equilibrium with melts having Mg# of >40 mol%. Although we do not dismiss the idea that *in situ* fractional crystallization can locally successfully reproduce–or, more realistically, contribute to–chemical zoning of the Cpx in gabbros (see also Bedard, 1994), this process requires an unfeasibly high amount of melt entrapment, which is markedly at odds with the mineralogy, texture and major element compositions of the evolved melt band in the current sample.
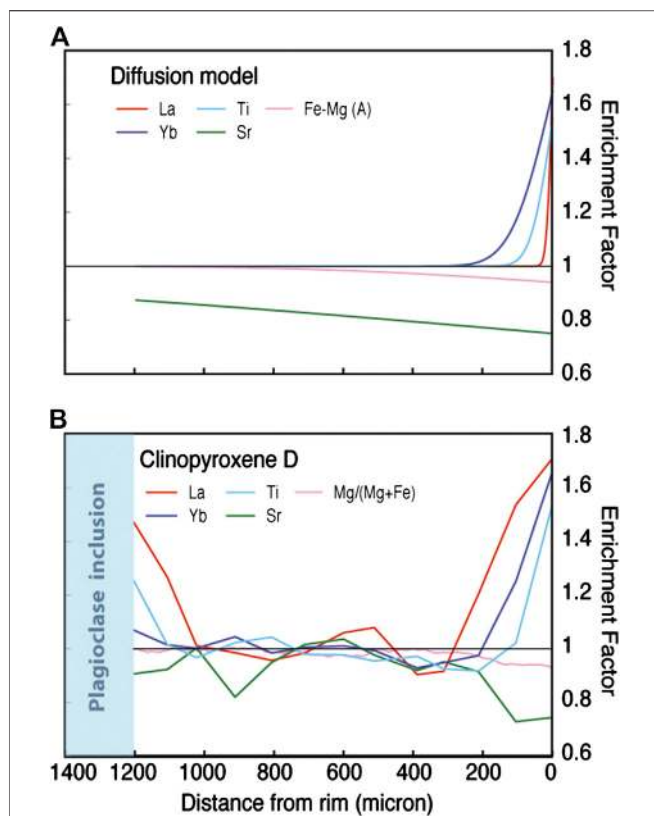
FIGURE 7 | Diffusion model **(A)** compared with trace element profiles of Cpx D **(B)**. Panel **(A)** models the diffusive influx of selected elements into Cpx from a surrounding melt. The resulting compositional profiles track the post-diffusion concentration C relative to the concentrations in the melt C0. An essential characteristic of this and all comparable diffusion models is the contrasting diffusion length generated for different elements. In panel B actual data for the compositional profiles of Cpx D are plotted as the "Enrichment Factor", which is the concentration at a given point of the profile divided by that of the crystal core (here set as the 600–800 μm interval), and directly comparable to C/C0 in Panel **A**. A critical observation in **(B)** is that, in marked contrast to essential requirement of the diffusion model, the different elements in Cpx D co-vary at the same places along the profiles, and that La varies over significantly larger distances than can be accounted for by diffusion.

Diffusion

Diffusion, given sufficient time, is capable of generating significant changes in trace element concentrations in minerals. Furthermore, because different trace elements migrate at different rates, trace elements may become fractionated from one another, effecting changes in their ratios. Some authors have suggested that diffusive re-equilibration may play a dominant role in controlling trace element distributions in oceanic gabbros (Coogan and O'Hara, 2015). Is such diffusion by itself capable of generating the fractionations we observe? In this section we explore whether diffusion can indeed explain the observed zoning in our sample.

We envisage two possible scenarios in which diffusion can play a role. The first is the situation in which evolved melts migrate into and/or become trapped within a more primitive crystal matrix. Over and beyond simple crystallization (see previous section), the melt may also exchange components with the host crystals through

diffusive processes: hence, to test this scenario, we assume that the clinopyroxene was initially unzoned and developed zoning as a result of diffusive exchange with a more evolved melt. This scenario was evaluated in detail by Gao et al. (2007) for the example of trace element zoning in clinopyroxene in a gabbroic rock from Atlantis Bank (ODP Hole 735B), and we apply a simplified version of their approach to the geochemical profile of Cpx D in sample 360-U1473A-84R-4, 118–122. In **Figure 7** we present diffusion profiles calculated on the basis of the following constraints: 1) that diffusion occurred at a temperature of 1,100°C: this temperature was calculated from the REE data for the rim of the crystal using the Cpx-Pl_{REE-Y} geothermometer of Sun et al. (2017; **Supplementary Figure S3**): in a diffusion scenario this represent the equilibrium temperature between melt and mineral, and hence it is the best estimate of the temperature at which the diffusion event took place; and 2) that diffusion operated over a timescale of 26.6 kyr: this we derived by dividing the
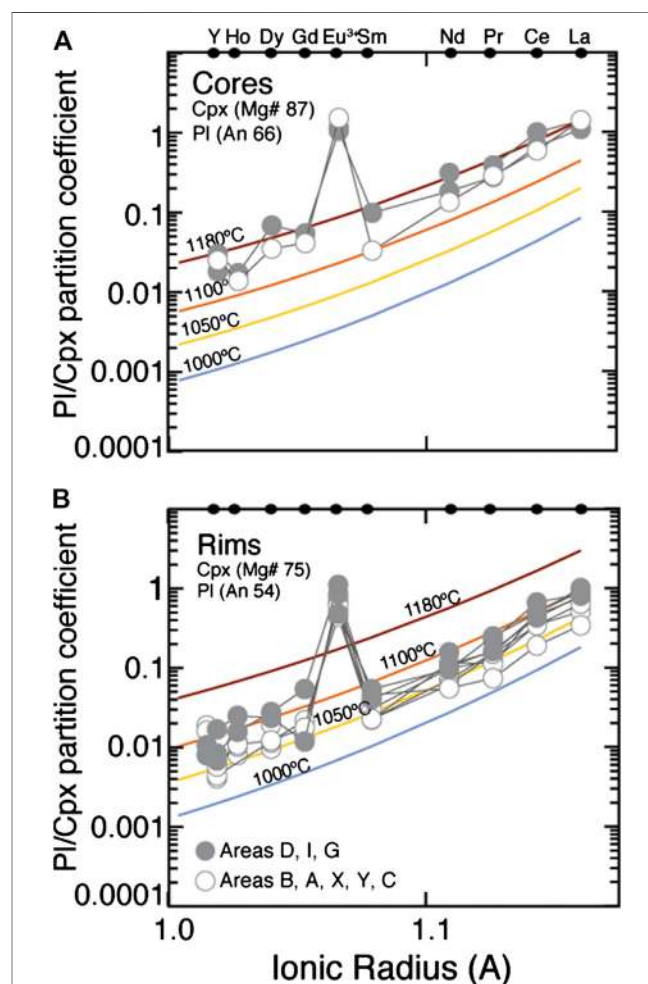

FIGURE 8 | Relationships between the Pl/Cpx trace element (Y and REE) ratios in the different areas of the studied rock and ionic radius. Equilibration temperature contour lines are calculated on the basis of the mineral major element compositions for core **(A)** and rim **(B)** compositions using the Pl/Cpx partitioning model developed by Sun and Liang (2012) and Sun et al. (2017).
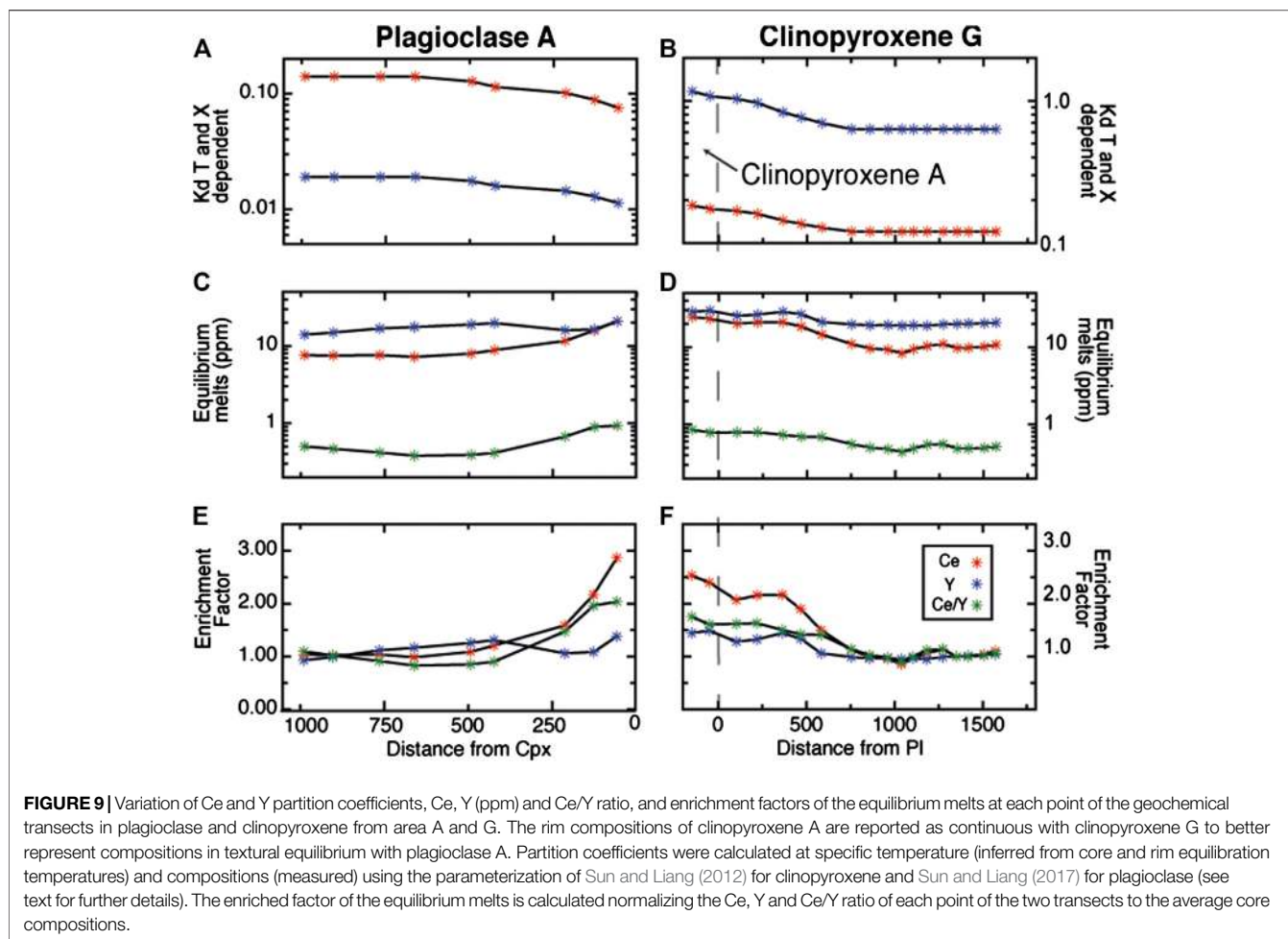
temperature interval of 77°C recorded by Cpx D (Cpx-Pl$_{REE-Y}$ temperature of 1,177°C for the core and 1,100°C for the rim; **Supplementary Figure S3**) by the cooling rate for Atlantis Bank gabbros (2,898°C/M.yr.; the average of cooling rates determined on 29 samples from ODP Hole 735B by Coogan et al., 2007). Although the use of combined geospeedometers suggests that the cooling rate of the Atlantis Bank decreases exponentially at temperatures <600°C (John et al., 2004), it may considered constant in the temperature interval considered here. Hence, the difference between "core" temperature, at which the Cpx initially crystallized from the melt, and the "rim" temperature provides an upper limit on the duration of the diffusion event. With the duration and temperature of diffusion thus constrained we were able to calculate the diffusion of La, Yb, Ti, Sr and Fe-Mg into the crystal using the Cpx diffusion data of Van Orman et al. (2001); REE, Cherniak and Liang (2012); Ti, Müller et al. (2013; Fe-Mg) and Sneeringer et al. (1984; Sr).

The results of the above modeling, shown in **Figure 7A**, provide a number of clear predictions that can be tested against real-world data (see also Gao et al., 2007). First, the diffusive influx of the REE is limited. This is particularly the case for La, which only diffuses ~20 μm into the Cpx (**Figure 7**). Second, because the diffusivity of the different elements differs substantially, their diffusion distances into Cpx vary significantly relative to one another. For example, among the REE, Yb migrates a factor of seven further into the crystal than La under the conditions modeled here. Fe-Mg, whose interdiffusion in Cpx is rapid (Müller et al., 2013) migrate further again (~1,200 μm), and Sr is affected by diffusion throughout the crystal (**Figure 7**). Diffusion will thereby lead to significant differences in zoning profiles for the different elements, and, consequently, fractionate element ratios significantly. Third, because individual REE have different diffusivities, these elements have different closure temperatures for diffusion (Dodson, 1973). Calculated REE closure temperatures for oceanic gabbros from ODP Hole 735B decrease systematically from 1,287°C for La to 1,135°C for Yb (Gao et al., 2007). Although these closure temperatures will vary depending on the assumed cooling rate, grain size and grain geometry, a decrease in closure temperature from LREE to HREE will be present in any particular diffusion scenario.

These three predictions (**Figure 7A**) can be tested against our observations, which we present in **Figure 7B**. Measured trace element profiles for Cpx D show that: 1) La enrichment occurs over a distance of >300 μm, much higher than that predicted for diffusion (**Figure 7B**); 2) enrichment becomes detectable at very similar distances along the profile for each and all of the elements: strikingly, it is clear that enrichment in the slowest-diffusing element considered here (La) occurs at the same location as the change in Mg#, which diffuses much more rapidly (**Figure 7B**); 3) The different REE all record very similar temperatures. This is illustrated in **Figure 8**, where we plot the ratios of the measured REE + Y concentrations in Pl vs. Cpx against their ionic radii. The observed Kds are compared to the Pl/Cpx Kds computed at major element compositions of Pl and Cpx akin to those of the mineral cores (Pl An 66; Cpx Mg# 87) and rims (Pl An 54; Cpx Mg# 77) and at temperature ranging from 1,180 to 1000°C. The Kd$^{REE}_{Pl/Cpx}$ of our Pl/Cpx couples form linear

correlations vs. the ionic radii, following those of the trends computed at constant temperatures (see also **Supplementary Figure S2**). Each of these observations allows us to rule out models in which diffusion plays a major control on the trace element concentrations, in keeping with previous deductions from ODP Hole 735B (Gao et al., 2007; Lissenberg and MacLeod, 2016).

A second diffusion scenario is one in which *in situ* fractional crystallization of interstitial melt is followed by sub-solidus diffusion between coexisting Pl and Cpx (Coogan and O'Hara, 2015). Modeling REE to diffusion between coexisting Pl and Cpx down to a closure temperature of 700°C, these authors argue that this scenario is capable of modifying the initial trace element profiles of oceanic cumulus minerals to such an extent that they control the observed variations in incompatible trace element zoning. A number of arguments may be made to show that this cannot be the case for our sample. The first is the REE equilibration temperatures recorded by our sample. We show above that the REE in Cpx D equilibrated at 1,177°C (core) and 1,100°C (rim). Extending this to all data from the sample we calculate REE equilibration temperatures for a series of Cpx-Pl pairs (**Supplementary Figure S1** and **Supplementary Tables S1, S2**), and derive estimates of the closure temperature using the Pl-Cpx trace element thermometer of Sun et al. (2017), calculating temperatures for each area in a traverse across the compositional band (**Figure 3**). Equilibrium temperatures for the selected Pl and Cpx rim couples range between 1,030 (±22)°C and 1,100 (±8)°C (see **Figure 3**). Using the same method we also calculate inferred core Pl and Cpx temperatures using core compositions in each area of the thin section, making the assumption that cores of physically adjacent cumulus minerals were in chemical equilibrium during their formation. Note that core temperatures could not be calculated for those locations within the compositional band because Cpx with "core" compositions do not occur. We find core temperatures to be rather uniform: in the range 1,156 (±5)°C to 1,181 (±12)°C. The relatively high equilibration temperatures of the rims, combined with the (very high) cooling rate of Atlantis Bank gabbros (Coogan et al., 2007), means that the sample did not have enough time at elevated temperatures to have suffered significant sub-solidus diffusion (Fig. 7). The second observation inconsistent with a sub-solidus diffusive control on the trace elements is that the closure temperatures for the different REE are all similar (see above, and **Figure 8**). Third, sub-solidus diffusion between Cpx and Pl leads to a number of distinct signatures in resulting trace element profiles (Coogan and O'Hara, 2015). Arguably the most obvious of these is that La will diffuse out of Cpx and into adjacent Plag, leading to a distinct decrease in Cpx La when approaching Plag (Coogan and O'Hara, 2015; their **Figure 4**). Cpx D provides an ideal test case for this prediction because, in addition to being in contact with plagioclase at its rim, the traverse also crossed into a plagioclase inclusion. From **Figure 7B** it is evident there is no decrease in La either at the crystal rim or near the inclusion. Rather, we infer that the high La contents of the Cpx close to the Pl inclusion was produced by an igneous process, either melt entrapment or melt-rock reaction (see below). We therefore conclude that the REE distributions in our samples are inconsistent with a sub-solidus diffusive control.
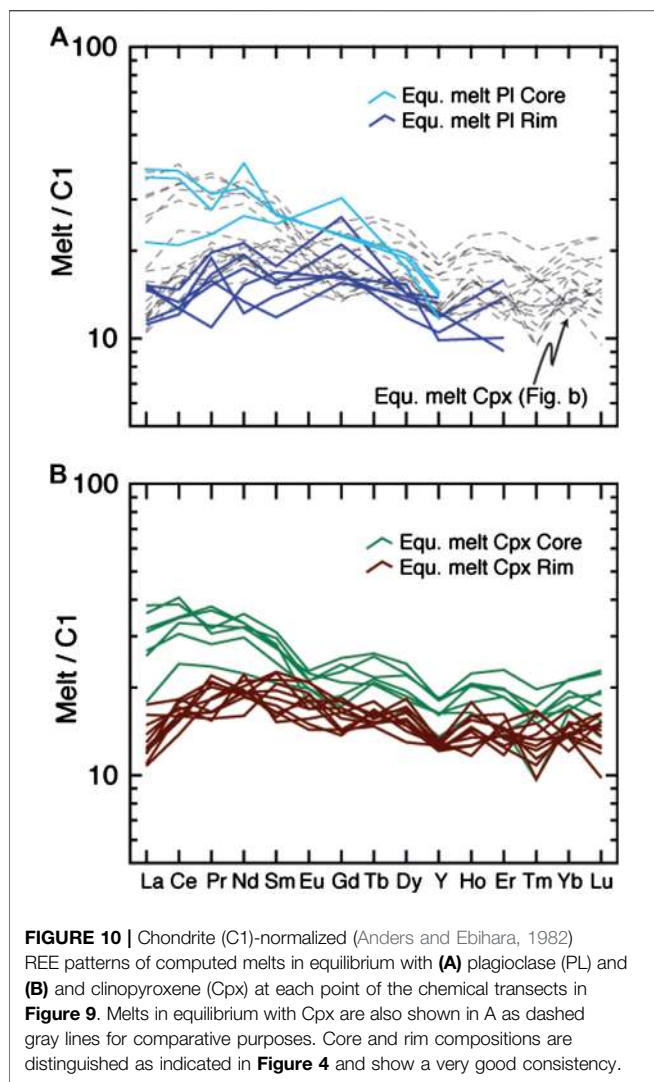
FIGURE 9 | Variation of Ce and Y partition coefficients, Ce, Y (ppm) and Ce/Y ratio, and enrichment factors of the equilibrium melts at each point of the geochemical transects in plagioclase and clinopyroxene from area A and G. The rim compositions of clinopyroxene A are reported as continuous with clinopyroxene G to better represent compositions in textural equilibrium with plagioclase A. Partition coefficients were calculated at specific temperature (inferred from core and rim equilibration temperatures) and compositions (measured) using the parameterization of Sun and Liang (2012) for clinopyroxene and Sun and Liang (2017) for plagioclase (see text for further details). The enriched factor of the equilibrium melts is calculated normalizing the Ce, Y and Ce/Y ratio of each point of the two transects to the average core compositions.

A further, independent, complementary consideration is the spatial distribution of crystal domains enriched in incompatible elements (**Figures 3, 4**). The element maps (**Figures 3B, 4**) reveal a great complexity to the chemical zoning: first, the enriched domains (illustrated by those areas with lower Mg# and An) do not only occur from core to rim but also vary across the sample; second, the enrichment is not necessarily simply related to its location (core to rim) within a single grain: i.e. zoning is not always concentric. For instance, Pl and Cpx from the internal portion of the reactive layer (points X and Y in **Figure 3C**) do not show a well-defined chemical zoning but are instead characterized by rim-like trace element compositions and element ratios (e.g., Ce/Y), and no evidence of intra-grain chemical gradients (**Supplementary Figure S1**). These observations even by themselves are inconsistent with simple diffusion; instead, together with our findings above, they indicate that both the spatial distributions of enrichment (**Figures 3, 4**) and the compositional trends (**Figures 4-6**) must be controlled by magmatic processes.

Reactive Porous Flow

Several previous authors have suggested that assimilation of the pre-existing gabbroic minerals coupled with crystallization of new phases during reactive porous flow (Coogan et al., 2000; Borghini and Rampone, 2007; Gao et al., 2007) is capable of generating a preferential increase in the most incompatible elements (Zr, Hf, LREE) compared to moderately incompatible elements (M-HREE, Y). This process is generally referred to as assimilation-fractional crystallization (AFC). AFC equations proposed by DePaolo (1981) have been employed successfully to reproduce the extent of fractionation in incompatible elements in abyssal gabbros (see also Lissenberg et al., 2013; Sanfilippo et al., 2015; Lissenberg and MacLeod, 2016). To test the hypothesis that chemical changes in the minerals in the band in our sample are produced by a reactive melt migration process we now consider a parameter referred to as the "enrichment factor" (EF; Lissenberg & MacLeod, 2016) as an aid to describing the intra-crystal chemical zonation. In any geochemical transect the EF is calculated as the composition of each point normalized to the crystal core composition. If the mineral-melt partition coefficients remained constant during the crystallization process, the EF of a given element in a mineral equals that of the equilibrium melt $\left(\dfrac{C_{point\ x}^{Sol}}{C_{Core}^{Sol}} = \dfrac{C_{point\ x}^{Liq} * Kd}{C_{Core}^{Liq} * Kd} \right)$. Temperature and composition are however known to have a major effect on mineral-melt partitioning; in particular, Sun et al. (2017) have
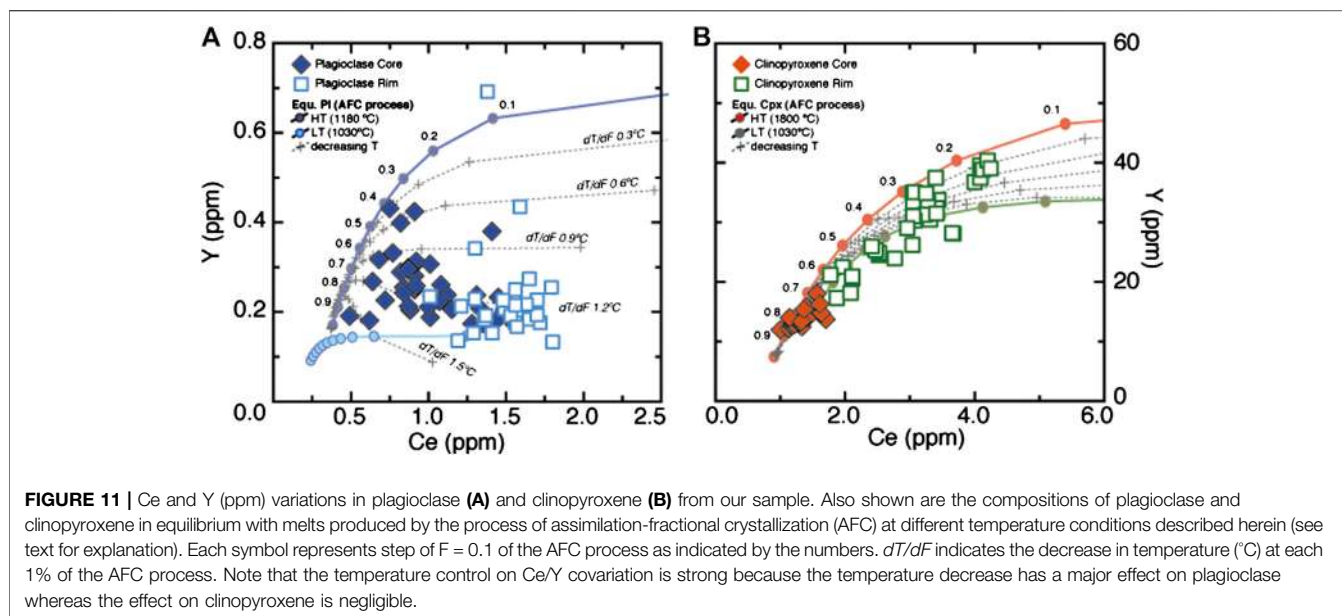
FIGURE 10 | Chondrite (C1)-normalized (Anders and Ebihara, 1982) REE patterns of computed melts in equilibrium with **(A)** plagioclase (PL) and **(B)** and clinopyroxene (Cpx) at each point of the chemical transects in **Figure 9**. Melts in equilibrium with Cpx are also shown in A as dashed gray lines for comparative purposes. Core and rim compositions are distinguished as indicated in **Figure 4** and show a very good consistency.

recently shown that the effect of temperature and composition on REE and Y partitioning in a basaltic system is particularly strong for Pl. This is shown in the **Supplementary Figure S3**, in which the variation in Pl-melt and Cpx-melt partition coefficients at temperatures between 1180° and 1,000°C are calculated using the average composition of Cpx-Core and Pl-Core (An 68, Cpx Mg# 87) and Cpx-Rim and Pl-Rim (An 57, Mg# 71). As discussed above, the REE + Y equilibration temperature reveals a difference of up to 150°C for the Pl and Cpx cores and rims (**Figure 3**).

On the basis of the formulations of Sun and Liang (2017) and Sun et al. (2017), and utilizing their mineral-melt partitioning models, we calculate the melt concentrations of the equilibrium melts at each point on each geochemical transect (**Figure 9**). To calculate the equilibrium melts we derived the mineral-melt partition coefficients from the major element composition and temperature at each point, using representative equilibration temperatures of 1180°C for Cpx-Core and Pl-Core, and 1050°C for Cpx-Rim and Pl-Rim. The results, shown in **Figures 9** and **10**, indicate that the REE and Y compositions of the equilibrium melts along the selected transects for Pl are very consistent with

those for Cpx when adjustments of the Kd for temperature and compositions are applied. In addition, the melts in equilibrium with Pl and Cpx Rims have similar EF for Y and Ce and, by consequence, reach similar Ce/Y ratios. We note that when the effect of temperature is considered, Y in the equilibrium melt displays a small, insignificant increase toward the rims of the crystal, whereas Ce increases sharply. Thus, even if the effect of temperature change in mineral-melt partitioning is taken into account, the Ce/Y ratios of the equilibrium melts still increase progressively toward the rims.

We will now explore whether melt-rock reaction can explain these variations. We opted for the assimilation-fractional crystallization (AFC) model based on the equations in DePaolo (1981). This model assumes that a proportion of solid is melted and incorporated into a transient melt that is simultaneously fractionating solid minerals. As assimilant, we used the average composition of Ol, Pl-Core and Cpx-Core at proportions derived from the modal proportions of these minerals in the sample (0.1:0.5:0.4), and a melt in chemical equilibrium with both Cpx- and Pl-Core as the initial melt. Crystallized phases were assumed to be only Pl and Cpx in nearly cotectic proportions (0.6:0.4), to account for the disappearance of Ol toward the compositional band. Mass assimilated vs. mass crystallized ratio was fixed at 0.99, which is consistent with the abundance of Cpx and Pl having "rim" like compositions in the compositional band compared to the less-modified host gabbro, indicating that assimilation and synchronous crystallization of new phases was highly efficient at least in the compositional band (details and parameters in **Supplementary Table S3** of supplements). In addition, the above analysis shows that the effect of temperature on partition coefficients is significant and must therefore be considered explicitly when modeling the evolution of incompatible elements. This being so, we calculate the composition of Cpx and Pl in equilibrium with melt evolving through an AFC process, using Kd that varies both for temperature and for major element composition. First, we derive two end member trends at constant temperature: the "high-T trend", calculated at temperature of 1180°C and major element compositions of the Cpx and Pl cores; and the "low-T trend", calculated at 1030°C and major element compositions of the Cpx and Pl rims (see **Supplementary Figure S3**). To bracket the range of possible temperatures derived from the Cpx-REE thermometry above we then consider a model characterized by a gradual decrease in temperature during the AFC process. At each step (arbitrarily fixed at F = 0.1), we decrease the temperature and modify the Pl and Cpx Kd accordingly. We varied the extent of temperature variation, i.e., decrease in temperature during the entire AFC process, progressively from 15°C to 150°C. This parameter, reported as *dT/dF* in **Figure 11** and **Supplementary Table S4**, indicates the magnitude of temperature decrease (°C) for each 1% of AFC process. This changes in response to the overall cooling of the system and, in a single sample, can reasonably be considered to be constant.

The results of our AFC model are shown in **Figure 11**, where the Ce and Y compositions of the Pl, Cpx and melts produced during an AFC process, both at fixed temperature and at varying

FIGURE 11 | Ce and Y (ppm) variations in plagioclase **(A)** and clinopyroxene **(B)** from our sample. Also shown are the compositions of plagioclase and clinopyroxene in equilibrium with melts produced by the process of assimilation-fractional crystallization (AFC) at different temperature conditions described herein (see text for explanation). Each symbol represents step of F = 0.1 of the AFC process as indicated by the numbers. *dT/dF* indicates the decrease in temperature (°C) at each 1% of the AFC process. Note that the temperature control on Ce/Y covariation is strong because the temperature decrease has a major effect on plagioclase whereas the effect on clinopyroxene is negligible.

temperature (gradually decreasing from 1180°C to 1030°C), are compared to those of our sample. In addition, we plot the trends resulting from fractional crystallization (Melt Entrapment) at temperatures decreasing to the same extent (i.e., 1180°C to 1030°C). Although in our model we focus on Ce and Y alone, these elements can be considered good representatives for the behavior of LREE and (M)HREE, respectively (see also Lissenberg and MacLeod, 2016). The model is satisfactory as the computed Pl and Cpx compositions mimic those in our sample and can potentially explain the relatively low Y at increasing Ce contents of the rim compositions of the selected minerals. The temperature decrease particularly affects the composition of Pl: we find the Pl of our sample is reproduced at 1.3°C of temperature decrease for each 1% of assimilation. This corresponds to an overall temperature decrease of 130°C during the entire process, which is of similar magnitude to the temperature drop estimated on the basis of the REE in Pl-Cpx thermometry in **Figure 3**.
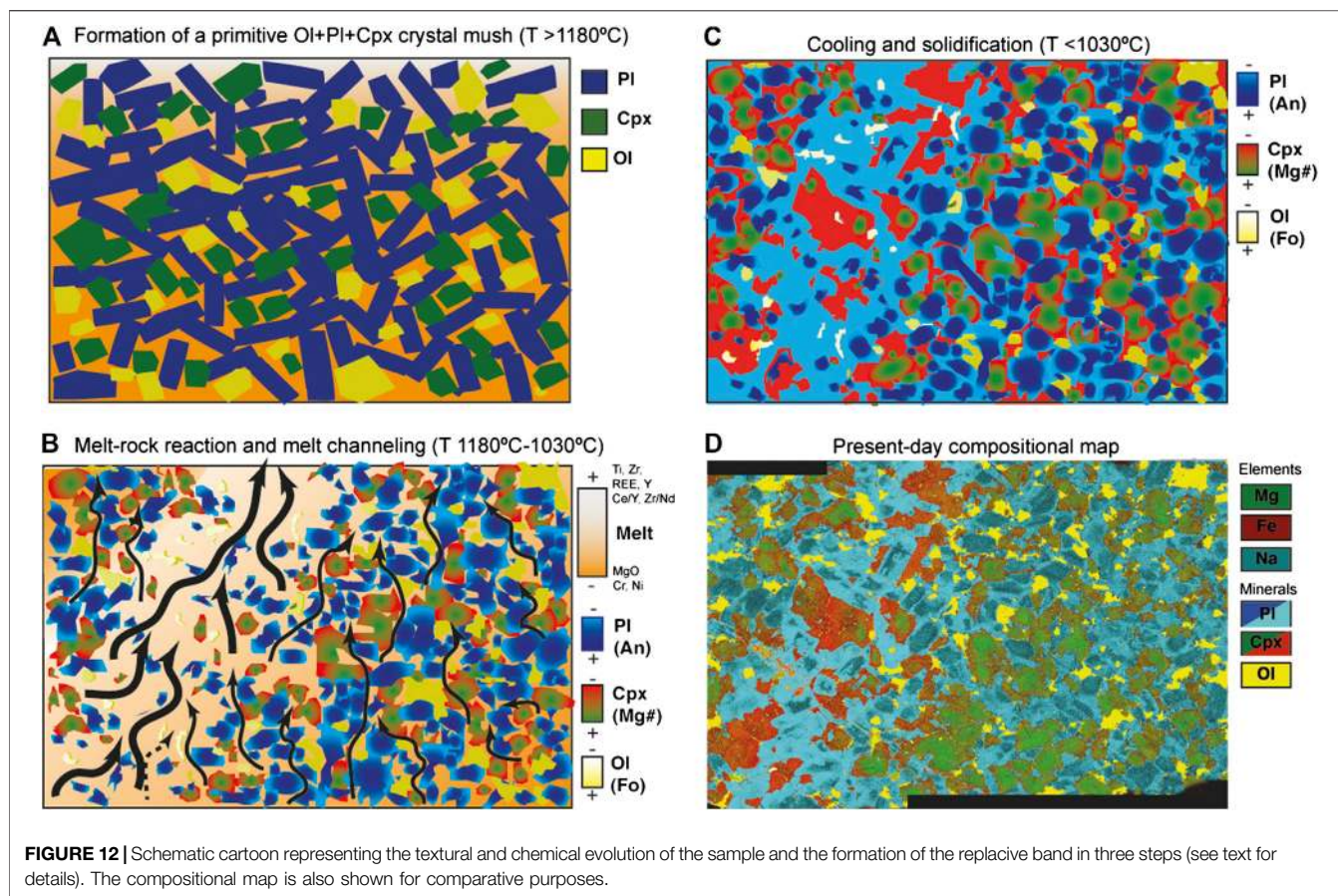
In conclusion, we demonstrate here that neither a process of closed system fractional crystallization with melt entrapment, nor modification by diffusion (be it supra- or subsolidus), can satisfactorily explain the major- and trace element chemical variations of the selected Pl and Cpx grains. Instead, we can successfully account for most of the broad variation in major and trace element compositions in our particular sample by a process of melt-rock reactions, at gradually decreasing temperature conditions, during the migration of an interstitial melt through a host crystal mush framework.

Origin of the "Compositional Band" and Possible Consequence for a Cryptic Reactive Porous Flow Process

The multi-element map (**Figure 3E**) shows the existence of a cm-size band otherwise undetectable on a purely petrological or microstructural basis (**Figure 3A**). Careful observation of this compositional band in petrographic thin section however shows that, in contrast to the remainder of the thin section, most Pl grains are characterized by An-rich cores with irregular shapes surrounded by thick Pl with more evolved, "rim-like" compositions. Chemical zoning is also observed in Cpx approaching the band, although Mg# zoning in Cpx seems smooth compared to other trace elements in the same traverse and corroded cores are not observed. This is potentially related to intercrystalline diffusion of Mg and Fe in Cpx, which may have slightly modified the original zoning due to a very high diffusivity of Fe and Mg in Cpx. In the previous sections we showed that neither melt entrapment nor diffusion can explain the trace element patterns of the selected Pl and Cpx in our sample, favoring the idea that chemical zoning was instead produced by a process of reaction between a former crystal matrix and migrating melt; hence, given that these enriched compositions are not only limited to the rims, but preferentially located toward and within the band, we infer a "replacive" origin for this band. On the basis of the presence within the band of "ghost" cores with compositions similar to those of the cores away from the band, coupled with the chemical dissimilarity between cores and rims, we suggest the band therefore most likely formed by the migration of an exotic melt into and through a pre-existing crystal framework rather than simply being residual liquid of the local crystal mush sucked or pressed out from the adjacent interstices. This process led to the partial to (locally) complete dissolution of a pre-existing Ol, Pl and Cpx framework, recrystallized into a newly formed Pl and Cpx assemblage.

Another fundamental observation is that the equilibration temperature of Pl/Cpx not only drops from core to rim of the same crystal, but that rim temperatures gradually decreases toward the reaction band, with a maximum temperature of 1100°C far from the reactive band and minimum estimate of ~1030°C in its medial portion (**Figure 3**). A reduction in

FIGURE 12 | Schematic cartoon representing the textural and chemical evolution of the sample and the formation of the replacive band in three steps (see text for details). The compositional map is also shown for comparative purposes.

equilibration temperature toward the band is consistent with thermodynamic models for reactive migration in porous media, which show that the average temperature of the system is gradually modified at the reaction front as consequence of the physico-chemical re-equilibration between the migrating melt and the crystals (Solano et al., 2014; Jackson et al., 2018). When an intergranular melt migrates through a porous mush the local bulk composition (i.e., the melt + solid compositions at each specific location along the reaction path) becomes more evolved along the melt transport pathway because of the gradual addition of melt, by definition enriched in the more fusible components. As a result, when reactive transport is considered, the temperature gradually decreases relative to the initial value at the migration front and the bulk composition becomes gradually more evolved. Although the major- and trace-element composition of the newly-formed phases and the disappearance of olivine in the reaction band suggest that the interacting melt was more evolved compared to that crystallizing the first generation of Pl and Cpx, the fact that the sample contains only a few grains of Ti-Fe oxide and Fe sulfide and no late-stage phases (amphibole, orthopyroxene or apatite), coupled with the higher An-in-Pl and Mg#-in-Cpx Rim compared to those in Ox-gabbros, indicate that it was nevertheless more primitive than those late-stage percolating melts that generated the Ox-gabbros that are otherwise prevalent throughout the Atlantis Bank gabbroic section (**Figure 1**; e.g., Dick et al., 1999; Pettigrew et al., 1999;

MacLeod et al., 2017). We deduce that the Ol-gabbro investigated here provides clear evidence that the primitive crystal mush formed at the earliest stages of generation of the Atlantis Bank lower crust experienced reactive melt migration from the outset, much earlier and not directly related to that associated with the later, much lower temperature Ox-gabbros (**Figure 1**). Instead, we propose that the percolating melt in the present case was the product of partial crystallization of the primitive liquid that formed the initial Ol-Pl-Cpx framework elsewhere in the same crystal mush pile, focused into the reaction band as it migrated, presumably upward, through the gradually cooling mush, most likely in response to compaction.

In **Figure 12** we summarize the processes of formation we deduce for the reaction band, which we conclude may be better described as a "reactive porous flow channel". We envisage this as a three-stage process. First of all a primitive crystal mush framework is formed by crystallization of a basaltic melt at temperature >1180°C, as defined by the equilibration temperatures of the Cpx-Pl mineral cores. The intergranular melts residual from this crystallization event started to migrate upward, likely driven by difference in buoyancy and/or compaction of the underlying cumulate pile. The chemical gradient between melts and crystals provoked interactions and the decrease in temperature conditions, leading to AFC processes and to a sharp increase in incompatible elements in the melt and in the newly formed crystals. As discussed above, the migrating melts were most likely residual after the

formation of the primitive crystal mush and became progressively undersaturated in olivine. In the same way as that inferred for replacive dunite channels in a partly molten mantle column (e.g., Spiegelman et al., 2001), the high solubility of olivine within the melt phase caused a positive feedback between dissolution and melt-flux, promoting the progressive focusing of these melts into a more permeable "replacive" channel. Here, most minerals crystallized from the migrating melt, leaving few, partly resorbed cores with original "core-like" compositions. Fast cooling of the gabbroic sequence likely due to exhumation in the detachment fault footwall (see John et al., 2004; Coogan et al., 2007; Rioux et al., 2016) led to the complete solidification of the crystal mush and the final equilibration of the mineral rims at nearly magmatic temperatures ($\geq 1030°C$); indeed, fast cooling rates likely inhibited further modifications by sub-solidus diffusion. Taken as a whole, the reactive melt migration process we document in this sample can thereby be regarded in microcosm as a snapshot of a general magmatic differentiation process, potentially occurring in other "homogeneous" olivine gabbros throughout the Atlantis Bank lower crust. By implication, we here demonstrate that interactions and reactions between melts and crystal mush happen from the earliest stages of intrusion and crystallization of the melts into a dynamic magmatic lower crustal system, as an inevitable consequence of the compaction, extraction and upward migration of interstitial melts throughout an early-formed primitive, cooling crystal mush.

SYNTHESIS

In this study we report the occurrence of cryptic reactive melt migration through a primitive crystal mush as preserved in olivine gabbros from deep within the plutonic lower crust of an ultraslow-spreading mid-ocean ridge. High-resolution chemical maps and trace element zoning profiles reveal cryptic chemical variations in the mineral phases, localized in particular in a discrete, cm-scale compositional band. Major- and trace element mineral compositions reveal the occurrence of well-defined Pl and Cpx trace element zoning profiles most likely produced during a process of dissolution-reprecipitation under decreasing temperature conditions. For the first time, we explicitly consider th effect of changes in mineral-melt partitioning that are a direct consequence of this temperature drop, and show that temperature-driven disequilibrium in and by itself is sufficient to account for the chemical changes in the newly-formed minerals and in the equilibrium melts. The preferential occurrence of these relatively more evolved mineral compositions within the compositional band suggests that the latter formed by a process of focusing and transport of interstitial melt through a crystal framework. The cryptic changes toward more evolved compositions and trace-element over-enrichment that are consequence of this process are impossible to detect on textural evidence alone but require sophisticated chemical mapping techniques

comparable to those presented herein. It is highly likely, therefore, that melt-rock reaction and reactive porous melt migration similar to that reported here is a far more important mechanism of chemical evolution of igneous rocks than hitherto recognized, and may potentially be responsible for a significant proportion of crystal and melt modification in magma reservoirs.

DATA AVAILABILITY STATEMENT

All datasets presented in this study are included in the article/**Supplementary Material**.

AUTHOR CONTRIBUTIONS

AS, CM, and RT conceived the project. CM chose the samples and ran the compositional maps, using the approach designed by JL. AS compiled the figures and performed the geochemical models. JL performed the diffusion model. AZ performed the LA-ICP-MS analyses. AS and CM wrote the text with the contribution of all authors.

FUNDING

ACKNOWLEDGMENTS

SUPPLEMENTARY MATERIAL

The Supplementary Material for this article can be found online at: https://www.frontiersin.org/articles/10.3389/feart.2020.579138/full#supplementary-material

REFERENCES

Anders, E., and Ebihara, M. (1982). Solar system abundances of the elements. *Geochem. Cosmochim. Acta.* 46, 2363–2380. doi:10.1016/0016-7037(82)90208-3

Beard, J.S., Ragland, P.C., and Rushmer, T. (2004). Hydration crystallization reactions between anhydrous minerals and hydrous melt to yield amphibole and biotite in igneous rocks: description and implications. *J. Geol.* 112, 617–621.

Bedard, J. H. (1994). A procedure for calculating the equilibrium distribution of trace elements among the minerals of cumulate rocks, and the concentration of trace elements in coexisting liquids. *Chem. Geol.* 118, 143–153. doi:10.1016/0009-2541(94)90173-2

Bédard, J. H., Hebert, R., Berclaz, A., and Varfalvy, V. (2000). "Syntexis and the genesis of lower oceanic crust," in *Ophiolites and Oceanic crust: new insights from field studies and the Ocean Drilling Program.* Editors Y. Dilek, E. M. Moores, D. Elthon, and A. Nicolas (Boulder, CO: Geological Society of America), Vol. 349, 105–119.

Blackman, D. K., Ildefonse, B., John, B. E., Ohara, Y., Miller, D. J., and MacLeod, C. J. (2006). "IODP expeditions 304 & 305 characterize the lithology," in *Proceedings of the Integrated Ocean Drilling Program.*, Vol. 304/305. (College Station, TX: Integrated Ocean Drilling Program.

Blackman, D.K., Ildefonse, B., John, B.E., Ohara, Y., Miller, D. J., Abe, N., et al. (2011). Drilling constraints on lithospheric accretion and evolution at Atlantis massif, Mid-Atlantic Ridge 30°N. *J. Geophys. Res.* 116, B07103. doi:10.1029/2010JB007931

Blum, P., MacLeod, C.J., Dick, H.J.B., Abe, N., Blackman, D.K., Bowles, J.A., et al. (2017). "Hole U1473A remediation operations, Expedition 362T," in *Proceedings of the International Ocean Discovery Program.* Editors C. J. MacLeod, H. J. B. Dick, P. Blum, and E. Scientists. (College Station, TX: International Ocean Discovery Program), 11.

Borghini, G., and Rampone, E. (2007). Postcumulus processes in oceanic-type olivine-rich cumulates: the role of trapped melt crystallization versus melt/rock interaction, *Contrib. Mineral. Petrol.* 154, 619–633. doi:10.1007/s00410-007-0217-5

Cannat, M., and Casey, J. F. (1995). "An ultramafic lift at the Mid-Atlantic Ridge: successive stages of Magmatism in serpentinized peridotites from the 15 degree N region," in *Mantle and lower crust exposed in Oceanic Ridges and in Ophiolites.* Editors R. Vissers and A. Nicolas (Norwell, MA: Kluwer), 5–34.

Cannat, M., Sauter, D., Mendel, V., Ruellan, E., Okino, K., Escartin, J., et al. (2006). Modes of seafloor generation at a meltpoor ultraslowspreading ridge. *Geology,* 34 (7), 605–608. doi:10.1130/G22486.1

Cherniak, D. J., and Liang, Y. (2012). Ti diffusion in natural pyroxene, *Geochem. Cosmochim. Acta.* 98, 31–47. doi:10.1016/j.gca.2012.09.021

Coogan, L. A., Jenkin, G. R. T., and Wilson, R. N. (2007). Contrasting cooling rates in the lower oceanic crust at fast- and slow-spreading ridges revealed by geospeedometry. *J. Petrol.* 48 (11), 2211–2231. doi:10.1093/petrology/egm057

Coogan, L. A., and O'Hara, M. J. (2015). MORB differentiation: *In situ* crystallization in replenished–tapped magma chambers. *Geochem. Cosmochim. Acta.* 158, 147–161. doi:10.1016/j.gca.2015.03.010

Coogan, L. A., Saunders, A. D., Kempton, P. D., and Norry, M. J. (2000). Evidence from oceanic gabbros for porous melt migration within a crystal mush beneath the Mid-Atlantic Ridge. *Geochem. Geophys. Geosyst.* 1. doi:10.1029/2000GC000072

Coogan, L.A., Thompson, G., MacLeod, C.J., Dick, H.J.B., Edwards, S.J., Hosford Scheirer, A., et al. (2004). A combined basalt and peridotite perspective on 14 million years of melt generation at the Atlantis Bank segment of the Southwest Indian Ridge: evidence for temporal changes in mantle dynamics? *Chem. Geol.* 207, 13–30.

Coogan, L. A., Wilson, R. N., Gillis, K. M., and MacLeod, C. J. (2001). Near-solidus evolution of oceanic gabbros: insights from amphibole geochemistry. *Geochem. Cosmochim. Acta.* 65, 4339–4357. doi:10.1016/s0016-7037(01)00714-1

Coumans, J. P., Stix, J., Clague, D. A., Minarik, W. G., and Layne, G. D. (2016). Melt-rock interaction near the Moho: evidence from crystal cargo in lavas from near-ridge seamounts. *Geochem. Cosmochim. Acta.* 191, 139–164. doi:10.1016/j.gca.2016.07.017

DePaolo, D. J. (1981). Trace element and isotopic effects of combined wall-rock assimilation and fractional crystallization. *Earth Planet Sci. Lett.* 53, 189–202. doi:10.1016/0012-821x(81)90153-9

Detrick, R. S., Buhl, P., Vera, E., Mutter, J., Orcutt, J., Madsen, J., et al. (1987). Multi-channel seismic imaging of a crustal magma chamber along the East Pacific Rise. *Nature.* 326, 35–41. doi:10.1038/326035a0

Dick, H. J. B., Kvassnes, A. J. S., Robinson, P. T., MacLeod, C. J., and Kinoshita, H. (2019a). The Atlantis Bank gabbro massif, Southwest Indian ridge. *Progress in Earth and Planetary Science.* 6, 64. doi:10.1186/s40645-019-0307-9

Dick, H. J. B., MacLeod, C. J., Blum, P., Abe, N., Blackman, D. K., Bowles, J. A., et al. (2019b). Dynamic accretion beneath a slow spreading ridge segment: IODP hole U1473A and the Atlantis Bank oceanic core complex. *J. Geophys. Res. Solid Earth.* 124, 12631–12659. doi:10.1029/2018JB016858

Dick, H.J.B., Meyer, P.S., Bloomer, S., Kirby, S., Stakes, D., and Mawer, C. (1991). "Lithostratigraphic evolution of an in-situ section of oceanic layer 3," in Proceedings of the Ocean Drilling Program, Scientific Results, 118. Editors R. P. Von Herzen, and P. T. Robinson (Station,TX: Ocean Drilling Program), 439–540.

Dick, H. J. B., Natland, J. H., Alt, J. C., Bach, W., Bideau, D., Gee, J. S., et al. (2000). A long *in-situ* section of the lower ocean crust: results of ODP Leg 176 drilling at the Southwest Indian Ridge. *Earth Planet Sci. Lett.* 179, 31–51. doi:10.1016/s0012-821x(00)00102-3

Dick, H. J. B., Natland, J. H., Miller, D. J., et al. (1999). *Proceedings of the Ocean Drilling Program, initial reports.* College Station, TX: Ocean Drilling Program, 176.

Dick, H. J. B., Ozawa, K., Meyer, P. S., Niu, Y., Robinson, P. T., Constantin, M., et al. (2002). "Primary silicate mineral chemistry of a 1.5-km section of very slow spreading lower ocean crust: ODP Hole 735B, Southwest Indian Ridge," in *Proceedings of the Ocean Drilling Program, scientific results.* Editors J. H. Natland, H. J. B. Dick, D. J. Miller, and R. Von Herzen (College Station, TX: Ocean Drilling Program), 176, 1–60. Available at: <http://www-odp.tamu.edu/publications/176_SR/chap_10/chap_10.htm>.

Dodson, M. H. (1973). Closure temperature in cooling geochronological and petrological systems. *Contrib. Mineral. Petrol.* 40, 259–274. doi:10.1007/bf00373790

Drouin, M., Godard, M., Ildefonse, B., Bruguier, O., and Garrido, C. J. (2009). Geochemical and petrographic evidence for magmatic impregnation in the oceanic lithosphere at Atlantis Massif, Mid-Atlantic Ridge (IODP Hole U1309D, 30°N). *Chem. Geol.* 264, 71–88. doi:10.1016/j.chemgeo.2009.02.013

Drouin, M., Ildefonse, B., and Godard, M. (2010). A microstructural imprint of melt impregnation in slow-spread lithosphere: Olivine-rich troctolites from the Atlantis massif (Mid-Atlantic Ridge 30°N, IODP Hole U1309D). *Geochem. Geophys. Geosyst,* 11, Q06003. doi:10.1029/2009GC002995.

Eason, D. E., and Sinton, J. M. (2009). Lava shields and fissure eruptions of the Western Volcanic Zone, Iceland: evidence for magma chambers and crustal interaction. *J. Volcanol. Geoth. Res.* 186, 331–348. doi:10.1016/j.jvolgeores.2009.06.009

Elthon, D., Casey, J. F., and Komor, S. (1982). Mineral chemistry of ultramafic cumulates from the North Arm Mountain Massif of the Bay of Islands ophiolite: evidence for high pressure crystal fractionation of oceanic basalts. *J. Geophy. Res.* 87, 8717–8734.

Ferrando, C., Godard, M., Ildefonse, B., and Rampone, E. (2018). Melt transport and mantle assimilation at Atlantis Massif (IODP Site U1309): constraints from geochemical modelling. *Lithos.* 323, 24–43.

Gao, Y., Hoefs, J., Hellebrand, E., von der Handt, A., and Snow, J. E. (2007). Trace element zoning in pyroxenes from ODP Hole 735B gabbros: diffusive exchange or synkinematic crystal fractionation?. *Contrib. Mineral. Petrol.* 153, 429–442. doi:10.1007/s00410-006-0158-4

Ghiorso, M. S., and Sack, O. (1995). Chemical mass transfer in magmatic processes. IV. A revised and internally consistent thermodynamic model for the interpolation and extrapolation of liquid-solid equilibria in magmatic systems at elevated temperatures and pressures. *Contrib. Mineral. Petrol.* 119 (2-3), 197–212. doi:10.1007/BF00307281.

Grimes, C. B., Cheadle, M. J., John, B. E., Reiners, P. W., and Wooden, J. L. (2011). Cooling rates and the depth of detachment faulting at oceanic core complexes: evidence from zircon Pb/U and (U-Th)/He ages. *Geochem. Geophys. Geosyst.* 12, 1–24. doi:10.1029/2010GC003391

Jackson, M. D., Blundy, J. D., and Sparks, R. S. J. (2018). Chemical differentiation, cold storage and remobilization of magma in the Earth's crust. *Nature.* 564, 405–409. doi:10.1038/s41586-018-0746-2

John, B. E., D. A., Foster, J. M., Murphy, M.J., Cheadle, A. G., Baines, C. M., Fanning, et al. (2004). Determining the cooling history of in situ lower oceanic crust-Atlantis Bank, SW Indian Ridge, *Earth Planet Sci. Lett.* 222, 154–160. doi:10.1016/j.epsl.2004.02.014

Koepke, J., Botcharnikov, R.E., and Natland, J.H. (2018). Crystallization of late-stage MORB under varying water activities and redox conditions: Implications for the formation of highly evolved lavas and oxide gabbro in the ocean crust. *Lithos.* 323, 58–77. doi:10.1016/j.lithos.2018.10.001

Koepke, J., Berndt, S.T.F., and Holtz, F. (2007). The formation of SiO2 rich melts within the deep oceanic crust by hydrous partial melting of gabbros. *Contrib. Mineral. Petrol.* 153 (1), 67–84. doi:10.1007/s00410-006-0135-y

Kvassnes, A.J.S., and Grove, T. (2008). How partial melts of mafic lower crust affect ascending magmas at oceanic ridge. *Contrib. Mineral. Petrol.* 156, 49–71.

Leuthold, J., Blundy, J. D., Holness, M. B., and Sides, R. (2014). Successive episodes of reactive liquid flow through a layered intrusion (unit 9, Rum Eastern Layered Intrusion, Scotland). *Contrib. Mineral. Petrol.* 168, 1021. doi:10.1007/s00410-014-1021-7.

Leuthold, J., Lissenberg, C. J., O'Driscoll, B., Karakas, O., Falloon, T., Klimentyeva, D. N., et al. (2018). Partial melting of lower oceanic crust gabbro: constraints from poikilitic clinopyroxene primocrysts. *Front. Earth Sci.* 6, 15. doi:10.3389/feart.2018.00015

Lissenberg, C. J., and Dick, H. J. B. (2008). Melt–rock reaction inthe lower oceanic crust and its implications for the genesis of mid-Ocean Ridge Basalt. *Earth Planet Sci. Lett.* 271, 311–325. doi:10.1016/j.epsl.2008.04.023

Lissenberg, C. J., and MacLeod, C. J. (2016). A reactive porous flow control on mid-ocean ridge magmatic evolution. *J. Petrol.* 57, 2195–2220. doi:10.1093/petrology/egw074

Lissenberg, C. J., MacLeod, C. J., and Bennett, E. N. (2019). Consequences of a crystal mush-dominated magma plumbing system: a mid-ocean ridge perspective. *Phil. Trans. R. Soc. A.* 377, 20180014. doi:10.1098/rsta.2018.0014

Lissenberg, C. J., MacLeod, C. J., Howard, K. A., and Godard, M. (2013). Pervasive reactive melt migration through fastspreading lower oceanic crust (Hess Deep, equatorial Pacific Ocean). *Earth Planet Sci. Lett.* 361, 436–447. doi:10.1016/j.epsl.2012.11.012

Loocke, M. P. (2016). The role of the axial melt lens in crustal accretion at fast-spreading mid-ocean ridges. PhD thesis. Cardiff (Wales): Cardiff University, 191.

MacLeod, C. J., Dick, H. J. B., Allerton, S., Robinson, P. T., Coogan, L. A., Edwards, S. J., et al. (1998). Geological mapping of slow-spread lower ocean crust: a deep-towed video and wireline rock drilling survey of Atlantis Bank (ODP Site 735, SW Indian Ridge). *InterRidge News.* 7 (2), 39–43.

C. J., MacLeod, H. J. B., Dick, and P., Blum, and theExpedition 360 Scientists (Editors) (2017). "in Southwest Indian Ridge Lower Crust and Moho." *Proceedings of the International Ocean Discovery Program.* (College Station, TX: International Ocean Discovery Program), 360.

Marjanovic, M., Carbotte, S. M., Carton, H., Nedimovic, M. R., Mutter, J. C., and Canales, J. P. (2014). A multi-sill magma plumbing system beneath the axis of the East Pacific Rise. *Nat. Geosci.* 7, 825–829. doi:10.1038/ngeo2272

Meyer, P.S., Dick, H.J.B., and Thompson, G. (1989). Cumulate gabbros from the Southwest Indian Ridge, 548S, 7816'E: implications for magmatic processes at a slow spreading ridge. *Contrib. Mineral. Petrol.* 103, 44–63.

Müller, T., Dohmen, R., Becker, H. W., ter Heege, J., and Chakraborty, S. (2013). Fe-Mg interdiffusion rates in clinopyroxene: experimental data and implications for Fe-Mg exchange geothermometers. *Contrib. Mineral. Petrol.* 166 (6), 1563–1576. doi:10.1007/s00410-013-0941-y

Natland, J. H., and Dick, H. J. B. (2001). Formation of the lower ocean crust and the crystallization of gabbroic cumulates at a very slowly spreading ridge. *J. Volcanol. Geoth. Res.* 110, 191–233. doi:10.1016/s0377-0273(01)00211-6

Nguyen, D., Morishita, T., Soda, Y., Tamura, A., Ghosh, B., Harigane, Y., et al. (2018). Occurrence of felsic rocks in oceanic gabbros from IODP Hole U1473A: implications for evolved melt migration in the lower oceanic crust. *Minerals.* 8, 583. doi:10.3390/min8120583

Ozawa, K., Meyer, P. S., and Bloomer, S. (1991). Mineralogy and textures of iron-titanium oxide gabbros and associated olivine gabbros from Hole 735B. *Proc. Ocean Drill. Progr. Sci. Results.* 118, 41–73. doi:10.2973/odp.proc.sr.118.125.1991

Pettigrew, T. L., Casey, J. F., Miller, D. J., et al. (1999). *Proceedings of the Ocean Drilling Program, Initial Reports.* College Station, TX: Ocean Drilling Program, 179.

Phipps Morgan, J., and Chen, Y. J. (1993). The genesis of oceanic crust: magma injection, hydrothermal circulation, and crustal flow. *J. Geophys. Res.* 98 (B4), 6283–6297. doi:10.1029/92jb02650

Renna, M. R., Tribuzio, R., Sanfilippo, A., and Thirlwall, M. (2018). Role of melting process and melt–rock reaction in the formation of Jurassic MORB-type basalts (Alpine ophiolites). *Contrib. Mineral. Petrol.* 173 (4), 31. doi:10.1007/s00410-018-1456-3

Rioux, M., Cheadle, M. J., John, B. E., and Bowring, S. A. (2016). The temporal and spatial distribution of magmatism during lower crustal accretion at an ultraslow-spreading ridge: high-precision U-Pb zircon dating of ODP Holes 735B and 1105A, Atlantis Bank, Southwest Indian Ridge. *Earth Planet Sci. Lett.* 449, 395–406. doi:10.1016/j.epsl.2016.05.047

Sanfilippo, A., Morishita, T., Kumagai, H., Nakamura, K., Okino, K., Hara, K., et al. (2015). Hybrid troctolites from mid-ocean ridges: inherited mantle in the lower crust. *Lithos.* 232, 124–130. doi:10.1016/j.lithos.2015.06.025Google Scholar

Sanfilippo, A., Morishita, T., and Senda, R. (2016). Rhenium-osmium isotope fractionation at the oceanic crust-mantle boundary. *Geology.* 44 (2), 167–170. doi:10.1130/G37428.1

Sanfilippo, A., and Tribuzio, R. (2013). Origin of olivine-rich troctolites from the oceanic lithosphere: a comparison between the Alpine Jurassic ophiolites and modern slow spreading ridges. *Ofioliti.* 38, 89–99. doi:10.4454/ofioliti.v38i1.418

Singh, S. C., Crawford, W.C., Carton, H., Seher, T., Combier, V., Cannat, M., et al. (2006). Discovery of a magma chamber and faults beneath a Mid-Atlantic Ridge hydrothermal field. Nature 442, 1029–1032.

Sinha, M. C., Constable, S. C., Peirce, C., White, A., Heinson, G., MacGregor, L. M., et al. (1998). Magmatic processes at slow spreading ridges: implications of the RAMESSES experiment at 57° 45′N on the Mid-Atlantic Ridge. *Geophys. J. Int.* 135, 731–745. doi:10.1046/j.1365-246x.1998.00704.x

Sinton, J. M., and Detrick, R. S. (1992). Mid-ocean ridge magma chambers. *J. Geophys. Res.* 97 (B1), 197–216. doi:10.1029/91jb02508

Sneeringer, M., Hart, S. R., and Shimizu, N. (1984). Strontium and samarium diffusion in diopside. *Geochem. Cosmochim. Acta.* 48, 1589–1608. doi:10.1016/0016-7037(84)90329-6

Solano, J. M. S., Jackson, M. D., Sparks, R. S. J., and Blundy, J. (2014). Evolution of major and trace element composition during melt migration through crystalline mush: implications for chemical differentiation in the crust. *Am. J. Sci.* 314, 895–939. doi:10.2475/05.2014.01

Spiegelman, M., Kelemen, P. B., and Aharonov, E. (2001). Causes and consequences of flow organization during melt transport: the reaction infiltration instability in compactible media, *J. Geophys. Res.* 106, 2061–2077. doi:10.1029/2000JB900240.

Suhr, G., Hellebrand, E., Johnson, K., and Brunelli, D. (2008). Stacked gabbro units and intervening mantle: a detailed look at a section of IODP Leg 305, Hole U1309D. *Geochem. Geophys. Geosyst.* 9. doi:10.1029/2008GC002012

Sun, C., Graff, M., and Liang, Y. (2017). Trace element partitioning between plagioclase and silicate melt: the importance of temperature and plagioclase composition, with implications for terrestrial and lunar magmatism. *Geochem. Cosmochim. Acta.* 206, 273. doi:10.1016/j.gca.2017.03.003

Sun, C., and Liang, Y. (2012). Distribution of REE between clinopyroxene and basaltic melt along a mantle adiabat: effects of major element composition, water, and temperature. *Contrib. Mineral. Petrol.* 163, 807–823. doi:10.1007/s00410-011-0700-x

Sun, C., and Liang, Y. (2017). A REE-in-plagioclase-clinopyroxene thermometer for crustal rocks. *Contrib. Mineral. Petrol.* 172, 24. doi:10.1007/s00410-016-1326-9

Tamura, A., Morishita, T., Ishimaru, S., Hara, K., Sanfilippo, A., and Arai, S. (2016). Compositional variations in spinel-hosted pargasite inclusions in the olivine-rich rock from the oceanic crust-mantle boundary zone. *Contrib. Mineral. Petrol.* 171 (5), 39. doi:10.1007/s00410-016-1245-9

Tribuzio, R., Tiepolo, M., Vannucci, R., and Bottazzi, P. (1999). Trace element distribution within olivine-bearing gabbros from the Northern Apennine ophiolites (Italy): evidence for post-cumulus crystallization in MOR-type gabbroic rocks. *Contrib. Mineral. Petrol.* 134, 123–133. doi:10.1007/s004100050473

Van Orman, J. A., Grove, T. L., and Shimizu, N. (2001). Rare earth element diffusion in diopside: influence of temperature, pressure, and ionic radius, and an elastic model for diffusion in silicates. *Contrib. Mineral. Petrol.* 141 (6), 687. doi:10.1007/s004100100269

Yang, A. Y., Wang, C., Liang, Y., and Lissenberg, C. J. (2019). Reaction between Mid-Ocean Ridge basalt and lower Oceanic crust: an experimental study. *Geochem. Geophys. Geosyst.* 20 (9), 4390–4407. doi:10.1029/2019gc008368